2003

Wood laminated composite poles

Cheng Piao
Louisiana State University and Agricultural and Mechanical College

WOOD LAMINATED COMPOSITE POLES

A Dissertation
Submitted to the Graduate School of the
Louisiana State University and
Agricultural and Mechanical College
In partial fulfillment of the
Requirements for the degree of
Doctor of Philosophy

in

The School of Renewable Natural Resources

by
Cheng Piao
B.S., Northeast Forestry University, 1987
M.S., Northeast Forestry University, 1990
M.S., Louisiana State University, 1998
May 2003

ACKNOWLEDGEMENTS

Numerous individuals provided invaluable help throughout this project, which can not be successfully completed without their invaluable assistance. I am sincerely grateful to Dr. Todd Shupe, my major professor, for his guidance, advice, and assistance. My deep appreciation is also extended to my other committee members. Specifically, I would like to express my sincere gratitude to Dr. Chung Y. Hse for his guidance and advice throughout this study. I am grateful to Dr. Vijaya Gopu, for his support and invaluable advice on numerous subjects. Dr. C. F. Niels DeHoop served as a committee member for my Master Degree and this degree and I would like to thank him for his assistance and support. I also appreciate Dr. Arnold Bouma for his critical review of this dissertation.

I wish to express my appreciation to Dr. R. C. Tang for his help and guidance on the test methodology of this project. Further appreciation is given to the following persons: Ms. Patricia Lefeaux and JoAnn V. Doucet for their various assistance, Xiaobo Li, Yaojian Liu, Dale Huntsberry, and Gary Smith for their assistance during the test of specimens, and Steve Johnson for providing testing equipment. I give my appreciation with fond memory to Dr. Elvin Choong for his support, assistance, and advice on this project.

I thank my wife, Xiru Yang, whose patience and support were a constant source of encouragement.

I am indebted to the Louisiana Forest Products Laboratory for funding this study and my assistantship at Louisiana State University.

TABLE OF CONTENTS

LIST OF TABLES

LIST OF FIGURES

ABSTRACT

Wood composite poles are new engineered products with polygonal shapes and bonded with synthetic resins. The poles have multiple advantages over the solid wood poles and are a promising solid pole substitute in power transmission, telecommunication, and cable TV services. The use of composite poles may reduce the cost both in materials and manipulation, and facilitate installation and treatment. It is necessary to evaluate the factors that affect their properties and construct theoretical and analytical models to analyze these properties.

Experiments were conducted to investigate strip thickness and number of strips' (NOS) effects on the flexural properties and shear stress of wood composite poles. Small-scale (diameter = 7.6 cm (3 in), length = 1.16 m (48 in)) and full size poles (diameter = 10.2 cm (4 in), length = 6 m (20 ft) were manufactured for this purpose. Four strip thickness levels and three number-of-strip levels for the small-scale poles, and three thickness levels and two number-of-strip levels for full-size poles were chosen as experimental variables. The lumber was cut into strips, which were bonded with synthetic resin in molds, and the resulting poles were evaluated in a cantilever test. Results show that the effects of strip thickness were negative on glue-line shear and positive on the shear at poles' clamped ends. But thickness had little effects on maximum bending stress of the small-scale poles and Young's modulus of both full- and small-scale poles. With the increase of NOS, Young's modulus of poles was increased. NOS had little effects on the maximum bending stress and glue-line shear of small-scale poles.

A theoretical analysis was carried out to study the deflection and stress of composite poles. Governing differential equations were derived from high-order differential equations based on the principle of minimum potential energy theorem. Transverse shear and body forces were included in the model. Investigations were also carried out to find glue-line effects on the stress and deflection of composite poles. An analytical solution is modeled with the finite element analysis using ANSYS. Both theoretical and analytical solutions were verified by the experimental data.

INTRODUCTION

The use of wood poles in communication systems dates back to 1844, when the first commercial telegraph system was constructed from Washington, D.C., to Baltimore, Maryland (Panshin et al. 1950). This marked the beginning of pole production in the forest-products industry. After about 40 years, poles were first used in another transmission system - the electrical power transmission lines. Wood poles are now widely used in communication and power transmission systems around the world. In 1998, about 130 to 150 million wood poles were used to carry overhead cables for electric, telephone and cables in the United States (Canadian Institute of Treated Wood (CITW) 1998). Both communication and electrical companies consume about two million wood poles in annual construction of new lines. One to two millions of poles are used to replace poles in service due to decay and/or mechanical damage (Erickson 1994).

Wood is an ideal material for poles. With the development of new materials and processing techniques, poles made from materials other than wood entered in the transmission and distribution markets. Spun concrete, light duty steel, and fiberglass are the three important sources of such materials. Since wood is subject to rot, decay and degradation from insects and woodpeckers, all of these materials are more durable than wood. Moreover, the weight of fiberglass poles is even lighter than wood poles. Nonetheless, wood is still the material of choice for poles in the U.S. This is due to the intrinsic attributes of wood. Compared to other poles materials such as steel and concrete, wood is produced from a renewable natural resource, which is resilient and extremely resistant to oxidation, corrosion, fatigue, crumbling, and spalling. If properly

preservative-treated, wood is protected against the biological agents that cause it to weaken and collapse in nature, namely: fungi and termites. Wood poles are easily climbed, more than adequately strong and easily machined. The decisive factor that wood is preferred over other materials is its low cost. Engineering Data Management Inc. (EDM) compared life-cycle costs of four types of poles (wood, light-duty steel, fiberglass (FRT), and spun concrete), and the results indicated that wood poles are the least expensive life-cycle choice in most distribution pole categories (AWPI, 1996). Although post-construction costs, such as inspection, maintenance, repair, replacement, and disposal, are higher, wood poles remain the cost-effective choice.

However, due to the ever-increasing population and demand for wood, logs that are suitable for transmission and distribution poles are becoming increasingly scarce. The availability of this pole-size timber has severely diminished (Marzouk et al. 1978; Miller and Graham 1970). On one hand, the wood pole industry faces the challenges of rising cost and losing market share. On the other hand, the power companies have tried to find a satisfactory substitute for the solid wood pole.

Orthotropic and laminated wood composite poles may be one of the solutions to the current pole resource problem. Wood composite poles consist of wood strips bonded with synthetic resin. The poles have polygonal cross-sections and a tapered form. Since the strip thickness is less than pole radius, composite poles are hollow inside. For a pole with a specific diameter, number of strips (NOS) and strip thickness are variables; for different applications, composite poles can be made into any diameter and length. Pole strips are normally finger- or butt-jointed to make them to pole length. The glue used is resorcinol-formaldehyde resin, which is weatherproof and can set at room temperatures.

There are multiple advantages of composite poles over solid wood poles. It normally takes 50 to 60 years for a tree to grow to a pole size. For composite poles, the strips can be materials of various ages and sources. Therefore, the material cost of composite poles is much lower than solid poles. The weight of hollow composite poles can be half or even less than that of solid wood poles. This not only reduces processing and transportation costs but also facilitates installation and transportation. In manufacturing composite poles, lumber from low-grade trees and recycled poles can be utilized. The disposal cost of solid poles can be greatly reduced by recycling into composite poles. Wood from plantation-grown trees, small diameter trees, short logs, crooked logs, and some processing residuals can be utilized as composite pole materials. For composite poles, preservative treatment is simple to be carried out. When solid poles are treated, since preservatives cannot reach the core, checks often occur during the service and shorten the service time. This situation is unlikely to happen to composite poles because of the size of the lumber and the permeability of plantation-grown wood (Choong and Fogg 1972; Tesoro and Choong 1976; Simpson et al. 1988).

It is believed that there is a potential market for this composite product. Utilization of low-grade timber bonded with high performance adhesives and fabricated using the optimal structural design will allow wood composite poles to have a great potential market and commercial values.

The objectives of this study are as followings:

1. Evaluate the mechanical properties of wood laminated composite poles.
2. Determine the factors that affect the mechanical properties of composite poles.

3. Develop theoretical and finite element models to predict the loading behavior properties of composite poles.

CHAPTER 1

LITERATURE REVIEW

Trees suitable for pole production must have long, straight, full-rounded boles with little taper. The materials that meet these requirements are from various species. Southern pine (*Pinus*, *sp*) is the main material for pole production in the nation. About 72 to 75 percent of poles are from this species (Koch 1972, Micklewright 1989). Other species for poles are western red and northern white cedars, Douglas fir, chestnut, Atlantic white cedar, bald cypress, and redwood (Panshin et al. 1950).

In the last decades, many new approaches have been designed to solve the pole-resource-shortage problem. Marzouk et al. (1978) used four design schemes to make shorter solid wood poles longer by splicing or strapping two to four shorter poles using steel connectors. They presented three types of splicing and frame poles that are structurally suitable substitutes for wood distribution power poles. They also investigated the possibility of making composite poles from wood and concrete in which the top position was made of pine and bottom position was made of concrete.

The concept of composite poles appears in 1981, when Adams et al. (1981) fabricated an innovative product using wood flakes, synthetic resin, and preservatives, and termed it the COMPOLE. The COMPOLE series are 40-foot long hollow poles with square, hexagonal, or octagonal cross sections. This was the first time that the concept of composite is applied in the field of wood poles. The poles they made are tapered from butt to tip according to the range found in solid wood poles. A computer program was used to design the poles and the optimal design they found was the poles that had a 7.5

cm (3 inches) wall thickness at a 33.8 cm (13.3 inches) ground-line diameter with the octagonal cross section. Shell thickness was reduced to 2.5 cm (1 in) at the top.

Hollow poles have advantages over solid poles. Since the poles are hollow, the poles are lighter in weight, which will save the cost in materials, shipping and installation, compared with that of solid poles. From a mechanical analysis standpoint, when a pole is subjected to a bending test, the bending stress is highest on the surface layer and zero in the center part of the pole due to the effect of moment of inertia. Ninety percent of a pole's bending strength is attributable to 22 percent of its diameter on both sides of the cross-section (Erickson 1995). Thus, taking some material from the center part will not significantly affect the service strength of poles. A conventional inspection method for poles in service also involves drilling to determine the shell thickness. A distribution pole is designated a reject if the pole shell thickness is 5 cm (2 in) or less (Wilson 1992). Examples like this can be found in the competitor to solid wood poles. Most of poles made of steel, concrete, and fiberglass are hollow inside.

Mechanical properties and weathering properties are obviously the two important factors that decided the application potential of COMPOLE. Krueger et al. (1982) reported that the average bending strength and modulus of elasticity (MOE) of aligned composite wood materials bound with isocyanate resin are 110.8 (16.1 x 10^3 psi) and 16,250 x 10^3 Pa (2.36 x 10^6 psi), which are higher than those of southern yellow pine. The weight of COMPOLEs, however, is 50 percent of the weight of solid wood poles of the same class and length (Adams et al. 1981).

Although weathering and biological attacks affect both COMPOLEs and solid wood poles, COMPOLEs are more vulnerable to these attacks. Since preservatives are

added to flakes before hot pressing, preservatives had detrimental effects on the initial strength properties of COMPOLEs. Test results showed that COMPOLEs lost some strength after weathering tests (Krueger et al. 1982). The COMPOLEs that contain inorganic salt-type preservatives had very high strength loss. They attributed the strength loss to the high temperatures used in the accelerated weathering test and predicted that the same results may not be seen in actual in-service weathering conditions. Wood composites are normally pressed at high temperature and humid environments. The built-in stress in the materials after pressed may release whenever it is possible. When COMPOLEs are in an in-service application environment, they will be subjected to constantly changes of moisture as well as temperature. The durability of COMPOLEs is a real concern.

Erickson (1994, 1995) proposed and patented a new design of composite poles. The hollow veneered pole (HVP) consists of a truncated strip cone with three or more overwraps of veneer layers. NOS in the cone could be 8 or whatever is most appropriate for the manufacture of a given sized pole. Each strip can be made from either random or standardized lengths of lumber, and can be finger-jointed to pole length. The overwraps are made of high strength softwood species veneer. Veneer grain direction is parallel to the pole axis. The function of veneer layers is to improve the bending strength and protect the glued surfaces of adjacent strips from weather.

There are no data reported about the mechanical properties of HVP. Since the strips in HVP are made from solid wood, it can be expected that HVP will have better mechanical properties and weathering ability than those of COMPOLE. Also the weight of HVP should be less than that of the same size of COMPOLE because the density of

structural composite materials is always higher than the density of wood material. All these make HVP an improvement on COMPOLE.

The wrapped veneer is the vulnerable part of the HVP. In the three-dimensional configuration of wood, the strength of the tangential direction is substantially lower than that of the longitudinal direction. When HVP swells due to the moisture changes in strips and veneer, the veneer-wrap is easily checked and peeled off and loses its utility. Furthermore, the over-wrap involves a complicated process of joining and gluing, especially when the pole is tapered. It is reported that the cost of over-wraps accounts for more than 20 percent of the total cost (Erickson 1994).

A merit of the substitutes to solid wood poles is sufficiently-strong strength and stability for tens of years in adverse environments. Both COMPOLE and HVP do not have these properties and may not be the most promising pole material. New designs are needed to solve the pole material shortage and work as the substitute for solid poles. One of the new designs is the wood laminated composite pole. In addition to the advantages that both COMPOLE and HVP have, wood laminated composite poles are more cost-effective, easier to make and be treated, more flexibility in sizes and shapes, especially, more durable than COMPOLE and HVP. Furthermore, in the theory of poles and beams, very few are found dealing with the hollow polygonal cross sections. The new design of composite poles has glue-lines and longitudinal connections. Few theories are available that take into account the effects of glue-lines and connections. Thus, a systematic study is obviously needed to assess the physical and mechanical properties of wood laminated composite poles. It is also imperative to develop theoretical and analytical models to facilitate the manufacture, installation, and maintenance of the composite poles.

1.1 References

American Society for Testing and Materials. 1996. Standard methods of static test of wood poles, D 1036-58(64).

American Institute of Timber Construction. Timber Construction Manual. 1974. John Wiley & Sons, New York. 928p.

Choong, E.T. and P.J. Fogg. 1989. Differences in moisture content and shrinkage between innerwood and outerwood of two short-leaf pine trees. Forest Prod. J. 39(3):13-18.

Canadian Institute of Treated Wood (CITW). 1998. Pole talk. Web address: www.citw.org/poletalk/.

Dougherty, J.J. 1985. Electrical systems division R&D report. Wood poles structure design. EPRI Journal Dougherty, J.J. 1985. Electrical systems division R&D report. EPRI Journal (3):47-51.

Koch, P. 1972. Utilization of the southern pines, Vol. 1, USDA For. Ser. Exp. Sta., Agric. Handbook 420, Washington DC. 1663p.

Micklewright, J.T. 1991. Wood preservation statistics. Proceedings of the American Wood-Preservers' Association 87:258-272.

Marzouk, H. M., M. U. Hosain, and V. V. Neis. 1978. Built-up utility poles using prairie timber. Forest Prod. J. 28(11):49-54.

Miller, D. J. and R. D. Graham. 1970. Durability of Douglas-fir hop poles treated with preservatives by diffusion. Forest Prod. J. 20(6):43-44.

Roliadi, H., C.Y. Hse, and E.T., Choong. 1996. Recycling of utility poles for useful engineered wood products. V.K.A. Gopu (Editor), Proc. 4th International Wood Engineering Conference, Vol. 1, pp. 454-461, Oct. 28-31, 1996, New Orleans, LA.

Roliadi, H. 1997. Recycling of utility poles for useful engineered wood products. Ph.D. Dissertation. Louisiana State University. Baton Rouge, LA. 201p.

Simpson, W.T., J.D. Danielson, and R.S. Boone. 1988. Press-drying plantation-grown loblolly pine 2 by 4's to reduce warp. Forest Prod. J. 38(11/12):41-48.

Tesoro, F.O. and E.T. Choong. 1976. Relationship of longitudinal permeability to treatability of wood. Holzforshung 30(3):91-96.

Wood Preserving Industry Production Statistical Report. 1996. American Wood Preservers Institute. 2750 Prosperity Avenue, Suite 550, Fairfax, VA22031.

Panshin, A.J., E.S. Harrar, W.J. Baker, P.B. Proctor. 1950. Forest products: their sources, production, and utilization. McGraw-Hill Book Company, Inc.

CHAPTER 2

MANUFACTURE AND EVALUATION OF COMPOSITE POLES

2.1 Introduction

Since the first use in the nineteenth century, wood is still the raw material of choice in today's distribution and communication pole market. However, with the diminishing availability of pole-sized trees, pole industries face a shortage of material and an increase in their cost. At the same time, the electrical and communication companies are trying to find substitutes for solid poles. Laminated wood composite poles are one important alternative for this purpose. These poles possess all the good properties the solid wood poles have, such as climbability and machinablity. The weight of composite poles is lighter than solid wood poles because the composite poles are hollow inside. The cost of composite poles is less than solid wood poles. From a mechanics stand point, if pole shell thickness is appropriate, hollow poles are still sufficiently strong to meet strength requirements. Ninety percent of a pole's bending strength comes from 22 percent of its diameter on both sides of the cross-section (Erickson 1995). Erickson proved that for a 12.2 m (40 ft) Class 4 hollow veneered pole (HVP), saving of wood could be 1/3 to 1/2 compared to solid poles. These properties make composite wood pole a potential product in the pole market.

There are two designs in the current research of composite poles. The first design uses wood flakes, synthetic resin, and preservatives to make poles (Adams et al. 1981). There are some similarities between the manufacture of composite poles of this kind and that of oriented strand board (OSB), in which the wood flakes with synthetic resin are

pressed under high temperature and pressure. Composite materials like this may store stress in the poles due to elevated temperature, humidity, and pressure applied to poles during manufacturing. The internal stress may be released whenever it is possible. The durability of the poles is a concern when they are introduced to the constantly changing outside environment. The second design consists of a wood strip cone over-wrapped by single- or multiple-veneer layers (Erickson 1994, 1995). The cone is composed of 8 or any appropriate number of strips (NOS), which are bound by synthetic resin side by side. The poles are hollow; thus, strip thickness may be a variable. The functions of veneer over-wraps were to protect the glue lines between strips and improve pole strength properties (Erickson 1995). Because the veneer is easily checked and peeled off from the poles, the over-wraps may not work as well as expected. The over-wraps account for about 20 percent of the total cost and involve a complicated process, especially when poles are tapered.

Wood laminated composite poles may be a better solution to the current problems that are related to the shortage of large diameter and long length wooden poles and beams. Laminated composite poles are thick-walled, polygonal shapes, and bamboo-like beams, as contrasted to solid poles and laminated veneer lumber (LVL). The objective of this part of study was to evaluate the factors that affect the physical and mechanical properties of composite poles. As a pre-study of full-size composite poles, small-scale poles were first made and tested. Full-size composite poles were made and tested based on the information obtained in small-scale poles. Effects of NOS and strip thickness on mechanical and water soaking properties were evaluated for both pole sizes.

2.2 Strip Size Determination

Strip size can be determined by mathematical calculation based on the parameters given. The known parameters are NOS in a pole $\boldsymbol{n}$, strip thickness $\boldsymbol{T}$, radius (or diameter) of the circle surrounding the bottom of a pole $\boldsymbol{R}$, tapering angle β, and pole height $\boldsymbol{H}$. Then the central angle α can be calculated as

$$\alpha = \frac{360^o}{n} \tag{2.1}$$

Other size measures can be determined by the relationship between sides and angles in a triangle. Figure 2.1 shows a schematic diagram about a composite pole and one of its strips. The formulas of other size are as followings:

Width of the larger size at pole bottom AB

$$\overline{AB} = 2R\sin\frac{\alpha}{2} \tag{2.2}$$

Width of the smaller size at pole bottom CD

$$\overline{CD} = 2R(\sin\frac{\alpha}{2} - T\tan\frac{\alpha}{2}) \tag{2.3}$$

Width of the larger size at pole top A'B'

$$\overline{A'B'} = 2(R - H\tan\beta)\sin\frac{\alpha}{2} \tag{2.4}$$

Width of the smaller size at pole top C'D'

$$\overline{C'D'} = 2(1 - \frac{H}{R}\tan\beta)(R - \frac{T}{\cos\frac{\alpha}{2}})\sin\frac{\alpha}{2} \tag{2.5}$$

Formulas 2.1 to 2.5 can be used to calculate the dimension of strips for a specific design of composite poles.

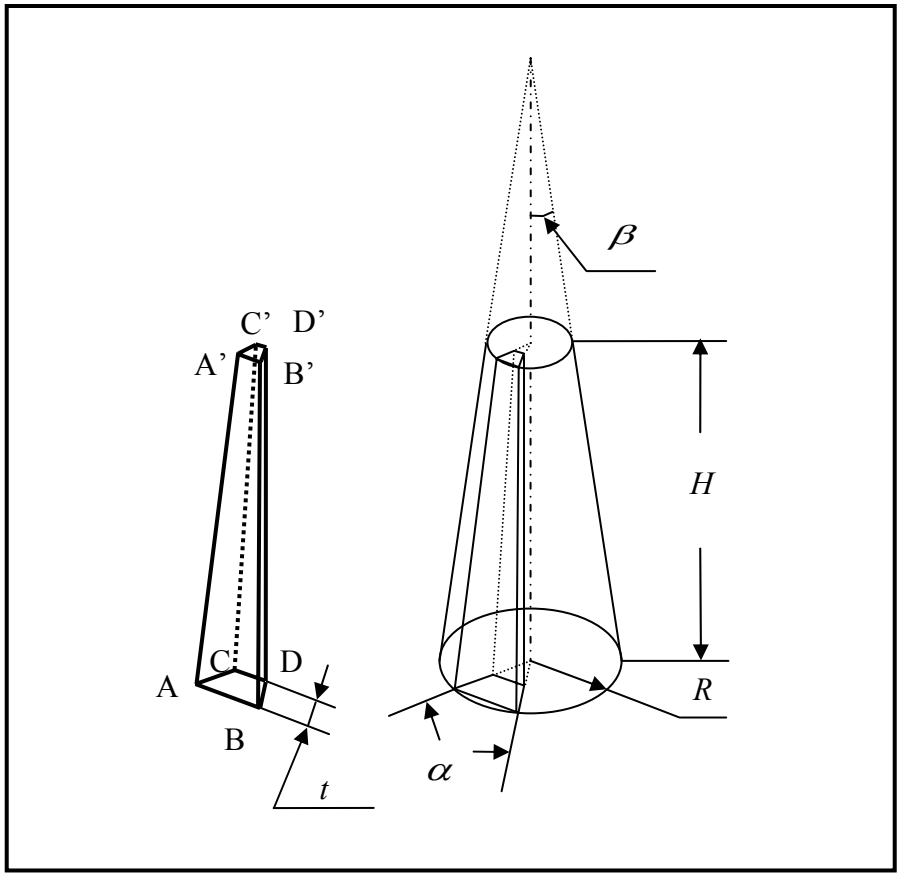

Figure 2.1. A schematic diagram of a wood strip composite pole and one of its strips.

If taper angle β equals 0, i.e., there are no tapers in the pole, Equations 2.4 and 2.5 are the same as Equations 2.2 and 2.3, respectively.

2.3 Experimental Procedure

2.3.1 Experimental Variables and Design

Poles made in this study had no taper. Table 2.1 shows the experimental variables and their levels. The small-scale poles (SSP) were used to simulate the properties of full-size poles (FSP) and two variables were selected for this purpose. Since strip thickness determines both strength properties and the cost, four and three levels were selected in the design of SSP and FSP, respectively. The thickness of the SSP accounts for 26, 39, 52, and 66 percent of the pole radius for strip thickness of 1.0 cm (0.4 in), 1.5 cm (0.6 in), 2.0 cm (0.8 in), and 2.5 cm (1.0 in), respectively. For FSP thickness accounts for 38, 56, and 75 percent of the pole radius for 1.9 cm (0.75 in), 2.9 cm (1.125 in), and 3.8 cm (1.5 in) strip thickness, respectively. Strip thickness covers one quarter to three quarters of pole radius in this study. Number of strips (NOS) was chosen as multiplications of 3 to facilitate calculations. SSP had three levels of NOS (6, 9, 12) and FSP had two (9, 12). Solid SSPs were used to compare the composite poles to solid wood and to compare the properties of different species. Two species were chosen, i.e., southern yellow pine and spruce. The cross section of the solid poles was 6-, 9-, and 12-side polygons for both southern yellow pine and spruce.

Table 2.2 presents the parameters for each NOS level of the strips with thickness 2.5 cm for SSP and 2.9 cm for FSP. The width of the larger side of other thickness levels is the same.

Table 2.1. Experiment variables and their levels of wood composite poles.

Pole Types	Species	Diameter (cm)	Length (cm)	Thickness Levels (cm)	Number of Strips
Small-scale composite	Southern yellow pine	7.6	122	1.0, 1.5, 2.0, 2.5	6, 9, 12
Small-scale solid	Spruce, southern yellow pine	7.6	122	------	6, 9, 12
Full-size composite	Southern yellow pine	10.2	610	1.9, 2.9, 3.8	9, 12

Table 2.2. Strip parameters of wood composite poles.

Pole Types	Number of strips	Central angle (^{o})	Strip thickness (cm)	Width of larger side (cm)	Width of smaller side (cm)
Small-scale poles	6	60	2.5	3.81	1.27
	9	40	2.5	2.61	0.87
	12	30	2.5	1.97	0.66
Full-size poles	9	40	1.5	3.47	0.87
	12	30	1.5	2.63	0.66

The experimental designs were factorial experiment designs for each experiment. The number of experiments was 12 for the small-scale poles and 6 for full-size poles. For RSP, thirty-six poles were made with 3 replications for each combination of NOS and strip thickness levels; For FSP, 12 poles were made with 2 replications for the NOS and strip thickness combinations. Three spruce and southern yellow pine poles were made for each of the 6-, 9-, 12-sided configurations. Nine spruce and nine southern yellow pine poles were used to test the properties of solid poles.

2.3.2 Materials and Methods

2.3.2.1 Specimen Preparation

Southern yellow pine (*Pinus*, *sp*) (SYP) lumber with sizes 5.08 cm by 15.36 cm by 6.1 m (2 in x 6 in x 20 ft.) and 5.08 cm by 20.32 cm by 6.1 m (2 in x 8 in x 20 ft.) was commercially obtained from a local store in Baton Rouge, Louisiana. Lumber pieces chosen were those that had no large (diameter > 1 cm) live knots and no dead knots. The lumber was randomly divided into two groups. One group was the materials for the RSP, and one for the FSP. The lumber for the SSP was cut into 125 cm (4.1 feet) pieces and reduced to target thickness with a planer. The lumber for the FSP was directly reduced to target thickness with the planer. The resulting lumber was cut into strips of specific target sizes using a table saw for both the SSP and FSP lumber pieces. The saw blade was turned to appropriate angles shown in Table 2.2 to form the target angles in strips. The cutting plan is shown in Figure 2.2. Strips may also be manufactured by first cutting lumber into a rectangle then shaping to appropriate angles. A comparison of this plan with the one shown in Figure 2.2 indicates that the latter may save some wood and require less labor.

Each strip was inspected for quality after the strip was cut from lumber. Strips with knots were removed and all strips were knot free. Strips were measured for weight, width of the larger side, and stress-wave properties. The stress-wave data were used in non-destructively assessing of the mechanical properties of poles. After measurement, the strips were stacked in a constantly air-conditioned room for two weeks before gluing into poles.

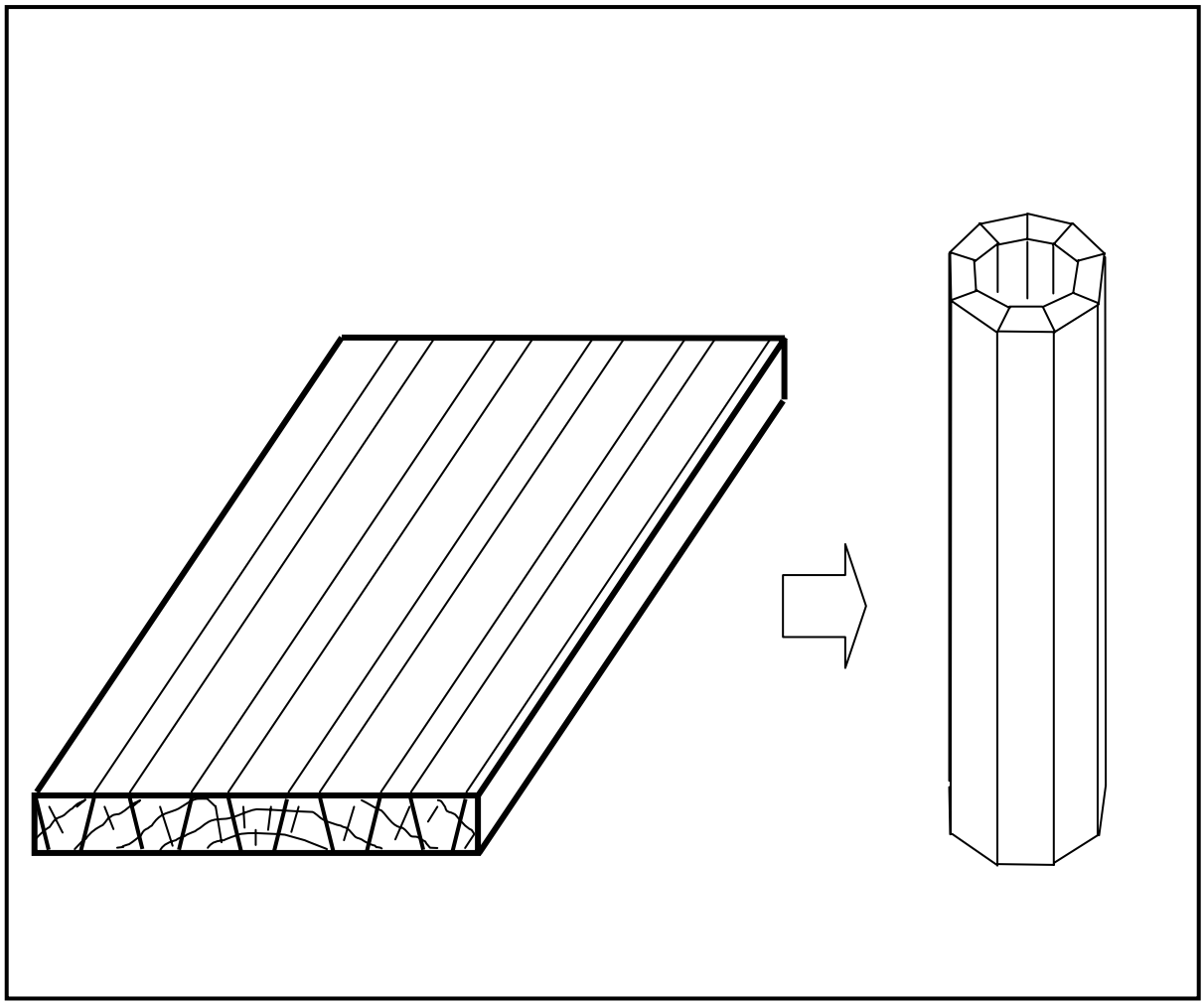

Figure 2.2. A schematic diagram of a strip-cutting plan for a nine-strip composite pole.

2.3.2.2 Manufacture of Composite Poles

The glue used in this study was resorcinol-phenol formaldehyde (RPF) resin and was commercially obtained from Borden Chemical, Inc. The viscosity and specific gravity of RPF were 800 cps and 1.177, respectively.

Strips that were assigned to a pole were randomly selected from one group of stacked strips for both SSP and FSP. Fifteen percent of setting agents was added to glue and the mixture was blended in a mixer. The ready glue was uniformly hand-spread onto the two side-surfaces at 310 g/m^2 (63.3lbs/1000 ft^2). Because both contacting surfaces had glue, some of the excess glue was squeezed out from glue lines after pressure was applied.

The consolidation of glued strips was performed in steel molds. The RSPs were pressed in a 137 cm (4.5 ft.) length steel mold, and FSP in a 640 cm (20 ft.) length steel mold. Glued strips were formed into a pole shape, tightened temporarily with tapes and then put into the lower half of a steel mold with 91.44 cm (3 inches) inside diameter. Rubber sheets were put in between poles and upper and lower halves of the steel mold. An impact wrench with 48.4 kg m (350 lbs ft.) of torque was used to tighten the screws on both sides of the steel mold. There were two functions of the rubber sheets. One was to prevent the poles from sticking onto the steel. The other one was to provide a buffer due to the pressure from steel to wood strips, and thus to prevent the mold from crushing wood strips.

Poles were pressed in molds for 36 hours in an air-conditioning room. Poles were then weighed and sanded. The poles were kept in an air-conditioned room for 4 weeks before testing.

2.3.2.3 Manufacture of Control Poles

To compare the properties of composite poles and to test the dynamic properties of solid wood poles, 6-, 9-, and 12-sided (polygonal) poles were made. Two materials were used. One was the same material as those of composite poles, i.e., the southern yellow pine; the other one was white spruce. Four pieces of 5.08 x 25.4 x 243.8 cm (2 in x 10 in x 8 ft.) SYP and spruce lumber were commercially obtained from the same source as the materials of the composite poles. The lumber was cut into 24 pieces of 5.08 x 7.6 x 121.9 cm (2 in x 3 in x 4 ft.) lumber. Two pieces of the lumber cut were bonded into square wood with dimension of 7.62 x 7.62 x 121.9 cm (3 in x 3 in x 4 ft.) using resorcinol-phenol-formaldehyde resin and 9 pieces of such square wood were obtained. Three of the 9 pieces of square wood were cut into 6-sided polygonal posts, three into 9-sided, and three into 12-sided posts for each species. The posts were kept in an air-conditioned room for 4 weeks before testing. To test the dynamic properties and facilitate the analysis of finite element of the solid poles, two strain gages were bonded onto the top and bottom surfaces 5 cm (2 in) away from the clamp end. The strain gages were connected to the Vishay's Model 6010 Strain Gage Input Card and the Model 6100 Scanner, which is connected to a computer.

2.4 Tests

2.4.1 Flexural Test

The flexural tests were conducted on SSP and FSP and performed on a REVEL machine. Before the test, the control system of the REVEL was replaced by a new digital system, which is controlled by a computer. Figure 2.3 shows the set-up of the test.

In Figure 2.3, one end of the tested composite pole B is fixed in the clamp of the supporting frame A. The pole was embedded 15 cm (6 in) in the clamp. The steel clamp was lined with the maple, which gripped the pole. Figure 2.4 shows the cross-section of the clamp, hard maple liner, and test specimen. The other end of the testing pole was tied to the crosshead E of the REVEL through a steel cable C and a pully D. When testing, the crosshead moved up along the spiral post F, imposing a concentrated load at the free end of the pole. The test was controled by computer H and the testing data are collected and stored in the computer.

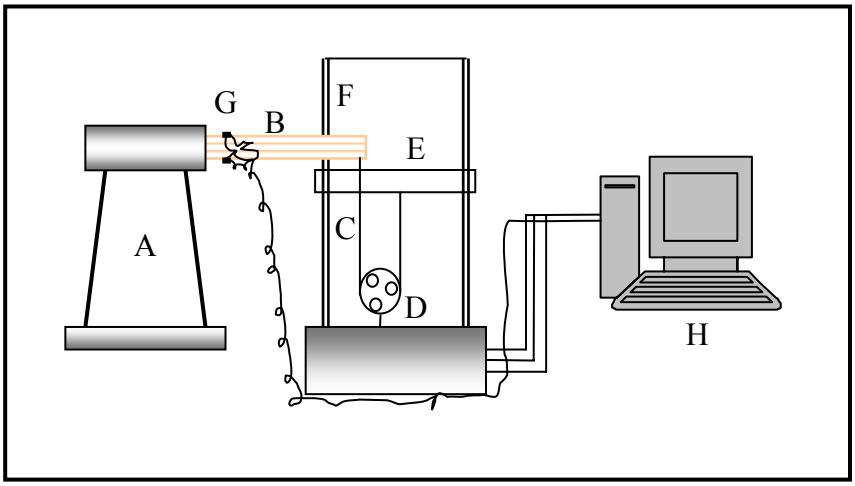

Figure 2.3. A schematic diagram of the flexural testing device.

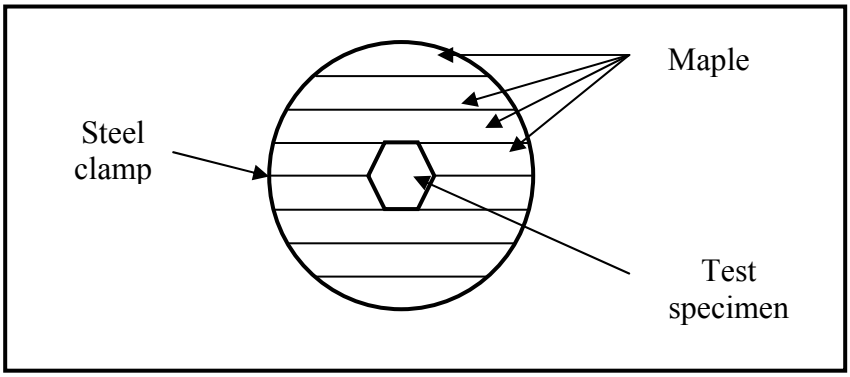

Figure 2.4. A schematic diagram of the clamp and the hard maple line used to grip the test specimen.

Strain gages on the pole B in Figure 2.3 were used to record strain in the bending test through software called StrainSmart. Figure 2.5 shows a strain gage attached to a solid spruce pole during a bending test. The software scanned the strain gages 1,000 times per second.

Figure 2.5. A strain gage was attached on the top skin of a small-scale spruce solid pole.

To enhance the crushing strength of FSP at the fixed end, the hollow part of the clamped end of each FSP was filled with thick plywood disks and glued particles. Two thick polygonal plywood disks with 1.25 cm (0.5 in) thickness were cut for each FSP. The disks were cut to fit the hollow part of each pole. Before the test, one disk was pushed into the poles to 91 cm (3 ft) and stopped by a 3-cm (1.2 in) nail that was driven in from the outside of the pole. The glued particles were then filled into the holes and rammed with a steel rod. After the hole was totally filled, the second disk with glue on

the particle side was pushed in to seal the hole. The glue used was resorcinol-phenol-formaldehyde resin. Resin content was 10 percent. After the operation, the poles were kept at room temperature for 36 hours before testing.

Static bending tests were carried out for both solid and composite poles. The experiment set-up is shown in Figure 2.3. Loading speed was 51 mm per minute (0.2 in/min). The length of the clamped end was 15.2 cm (6 in) for all the SSP and the length of the FSP at the clamped end was 91.4 cm (3 ft). Peak load and deflection values were recorded. The SSPs were tested twice. In the first test, all samples failed at the clamped end, where the pole was split in the central plane. After the first test, the clamped ends of the tested samples were removed. In the second test, the clamped length was increased to 30.5 cm (1 ft) and each sample was loaded to failure to obtain the maximum bending stress. In the test of FSPs, strain gages were mounted on top and bottom skins near the ground line and were used to measure strain during the loading process. FSPs were not loaded to failure due to the subsequent experiment on the poles and were tested to obtain only the modulus of elasticity (MOE). All FSPs were loaded to about 350 N (80 lbs) and the test was halted. Load values and corresponding deflection and strain were recorded. MOE was calculated from the load-deflection graph. Figure 2.6 shows a full-size composite pole in the bending test. Table 2.3 gives the information of the bending test for both small- and full-size poles.

After the second test on SSP, a sample was cut from the clamped end of each pole. The samples were measured for weight and then put in an oven at 100^{o}C for 24 hours. The moisture content at test was calculated based on the weight of the samples before and after oven-drying.

Table 2.3. Failure styles of solid and composite poles in a cantilever bending test.

TYPES OF POLES			NUMBER OF POLES	FIRST TEST	SECOND TEST
Small-scale poles	Composites	1.0 cm	9	Shear[1]	Shear
		1.5 cm	9	Shear	Shear
		2.0 cm	9	Shear	Normal[2]
		2.5 cm	9	Shear	Normal
	Solid	SYP	9	Normal	-----
		Spruce	9	Normal	-----
Full-size poles	Composites	1.9 cm	4	Non-destructive[3]	-----
		2.9 cm	4	Non-destructive	-----
		3.8 cm	4	Non-destructive	-----

[1] Shear failure at the clamped end.
[2] Normal failure at the ground-line.
[3] Loaded to about 350 N (180 lbs) and halted.

Figure 2.6. A full-size composite pole is loaded by a REVEL machine.

2.4.2. Glue-line Shear Test

After the bending test of each small-scale composite pole, the part measured 20 cm (8 in) from the clamped end of the pole was cut and kept for records. Four more samples measuring 5 cm (2 in) each were cut from the same end and used for the glue-line shear test. As shown in Figure 2.7, each sample was first cut into two halves. One glue line was randomly selected from each of the halves. The laminations on both sides of the glue line were reduced to 4.4 cm (1¾ in). Two of the samples were used to determine the glue-line shear in the dry condition. The samples were kept in an air-conditioned room for two weeks and tested to failure. The maximum load and wood failure of each sample were recorded.

The other two samples for each pole were used to test in wet conditions. The samples were put in a container measuring 36 x 72 x 23 cm (14 x 28 x 9 in). Water in the container was heated to 50^{o}C and the samples were put 2.5 cm (1 in) below the water surface using a net. The water was heated to boiling point in two hours and samples were kept in the boiling water for another two hours. At the end of the boiling test, the samples were taken out and immediately put in plastic bags. After the samples cooled to the ambient temperature in the bags, they were shear-tested to failure. The load to failure and percentage of wood failure on the glue-line were recorded. The load values in the wet condition and glue-line dimensions in the dry condition were used to calculate the shear strength for each sample.

A standard apparatus was used to hold the samples and an Instron machine was used to add the load. Before the test, each glue line in each sample was labeled, and measured for length and width. Then the glue lines in the sample were tested to failure.

The testing procedure is similar to the standard ASTM D 1037 Glue-Line Shear Test procedure except that the width of the samples was narrower because of the limited shell thickness of the poles. The shear stress at failure was calculated based on the maximum load and the glue line area, and the percentage of wood failure for each specimen was recorded after the test.

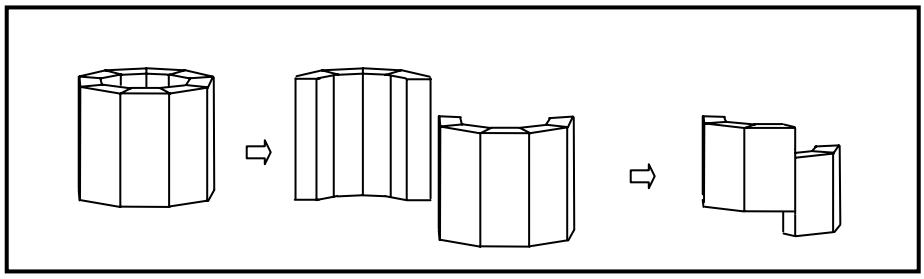

Figure 2.7. A schematic diagram of a sample cutting plan for the glue-line shear test.

2.5. Results and Discussion

2.5.1 Bending Stress

In the first bending test, SSP samples were shear-broken at the clamped end. It indicates that shear-failure may be an important failure mode for the hollow poles. Therefore, some other materials may be needed to fill the void part and withstand the shear effects.

The shear stress was calculated and Figure 2.8 and Table 2.4 show the results. The shear values for the small-scale poles were normally higher than the wood itself. This was due to the fact that the clamped end was pressed by the maple wood mold. As shown in Figure 2.8, except for the 12-sided poles in the 2.0 and 2.5 cm groups, the thickness of the poles had little effects on the shear stress of the poles.

Table 2.4. Shear stress of wood laminated composite poles in the cantilever bending test.

Strip Thickness (cm)	Shear Stress (MPa)		
	6	9	12
1.00	9.04 (0.17)*	9.69 (0.34)	9.79 (1.52)
1.50	8.11 (0.72)	11.81 (0.16)	10.34 (1.10)
2.00	8.22 (0.81)	10.42 (0.19)	13.47 (1.06)
2.50	8.32 (0.12)	11.45 (0.70)	12.44 (1.90)

* Values in parentheses are standard deviation.

Statistic analysis was conducted to analyze the effects of strip thickness and number on the shear stress of composite poles. NOS had significant effects on the shear stress at the clamped end ($p = 0.001$), but strip thickness showed no effects on the shear stress ($p = 0.15$). The average shear stress values of 12 samples of each number-of-strip level were 8.4, 10.8, and 11.5 MPa for 6-, 9-, and 12-sided poles, respectively. Least significant difference (LSD) procedure was used to compare the effects among different strip thickness and number-of-strip levels. This procedure is more conservative than other procedures such as Tukey and Scheffe, i.e., LSD may differentiate small differences caused by different levels in a variable. The shear stress was significantly lower than those of other two number-of-strip levels. The average shear stress values were 9.5, 10.1, 10.7, and 10.7 MPa for poles with 1.0, 1.5, 2.0, and 2.5 cm of strip thickness, respectively.

To test the bending stress of the small-scale poles, the clamped end of the pole tested was removed after the first test and the poles were tested again. In the second test, the clamped end was increased to 30.5 cm (12 in). Table 2.5 lists the results. In the test, all poles in the 1.0 and 1.5 cm of thickness levels were failure by shear at the clamped end, and poles in the other two thicker levels were failure at the ground line. There was

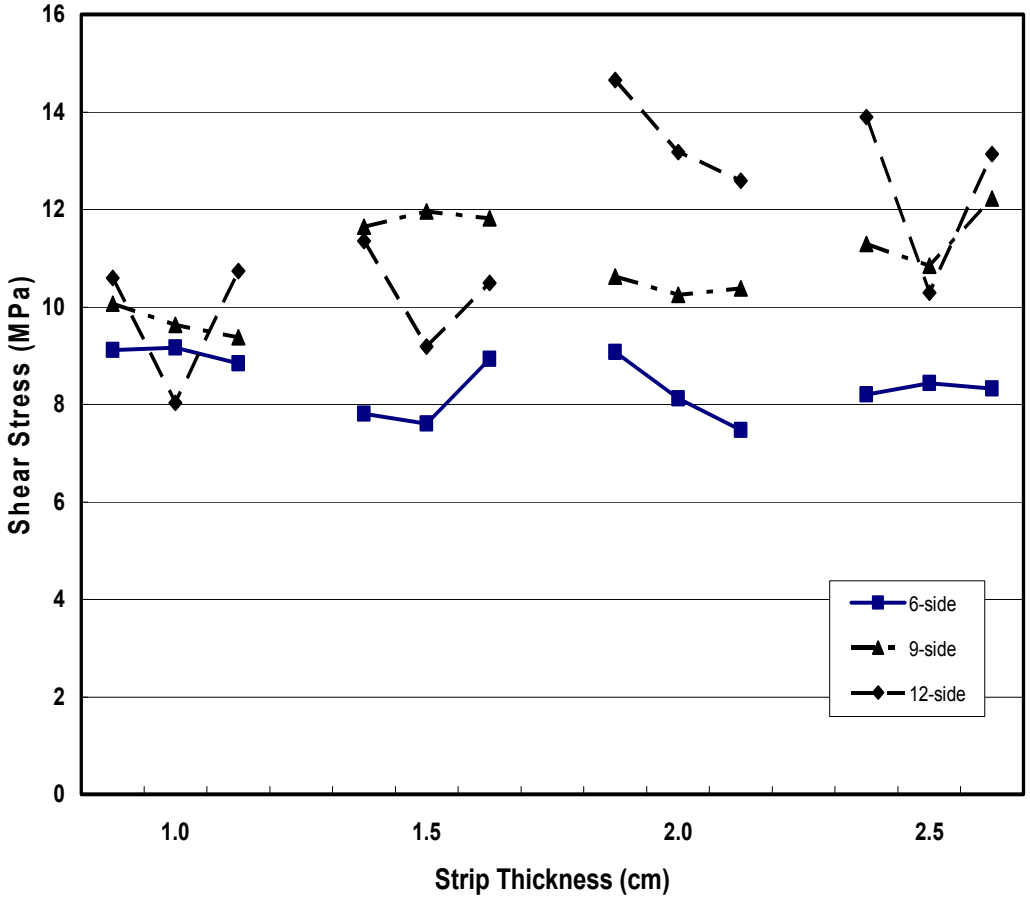

Figure 2.8. Effects of strip thickness and number of strips on the shear stress of small-scale wood composite poles.

little difference in the bending stress for different strip thickness and number levels. Although the two thinner shell poles were failure at shear, the shear stress values were listed in Table 2.5 due to the small difference between the shear stress values of the thinner poles and normal stress values of the thicker poles.

Table 2.6 lists the flexural properties of spruce and southern yellow pine solid poles that were bonded by two pieces of lumber and processed to polygonal shapes. The strength of the composite poles was comparable to that of bonded solid poles. In the 2.0 cm groups, the strength of 6-, 9-, and 12-sided poles accounted for 99, 82, and 90 percent of corresponding solid ones, respectively.

Table 2.5. Maximum bending stress of small-scale wood laminated composite poles.

Strip Thickness (cm)	Bending Stress (MPa)		
	6-strip	9-strip	12-strip
1.0*	96.27 (1.16)**	91.85 (1.68)	52.91 (6.27)
1.5*	96.76 (5.69)	90.02 (0.89)	80.53 (5.23)
2.0	101.37 (7.64)	80.84 (1.27)	99.46 (5.98)
2.5	106.16 (1.34)	108.86 (5.56)	97.80(12.53)

* The poles in these two thickness levels failed in shear at the clamped end.

** Values in parentheses are standard deviation.

Table 2.6. Flexural properties of the small-scale solid poles.

Species	MOR (MPa)			MOE (10^9Pa)		
	6-sided	9-sided	12-sided	6-sided	9-sided	12-sided
Spruce	61.59(13.65)*	68.06 (4.38)	72.87 (1.15)	5.35 (0.744)	6.42 (0.758)	6.24 (0.786)
SYP**	112.4 (2.15)	99.19 (4.37)	110.7(5.51)	8.12 (0.593)	7.95 (0.062)	7.65 (0.455)

* Values in parentheses are standard deviation.

** Southern yellow pine

2.5.2 Modulus of Elasticity

The Young's modulus values of small-scale composite poles of different strip thickness and NOS levels are presented in Table 2.7. Table 2.6 lists the modulus of spruce and southern yellow pine solid poles. Variations existed among different NOS and strip thickness levels in the MOE of composite poles, as shown in Figure 2.9. In general, the Young's modulus of composite poles was lower than those of solid poles with the same species. The reduction ranged from 0 up to 60 percent. Errors existed when prepared the strips that composed the poles. The integrity of the poles might thus be affected and a reduction in stiffness could be expected. Statistical results show that strip thickness was not correlated to the MOE values of the composite poles ($p = 0.3928$). The average MOE values were 6.2, 6.6, 5.7, and 5.9 TPa for strip thickness of 1.0, 1.5, 2.0, and 2.5 cm, respectively. There were no significant differences among the MOE values in the LSD test.

Table 2.7. Modulus of elasticity of small-scale wood laminated composite poles.

Strip Thickness (cm)	MOE (10^9Pa)		
	6-strip	9-strip	12-strip
1.0	5.77(0.59)	4.73(0.31)	6.49(1.02)
1.5	5.32(2.33)	6.49(0.82)	6.45(1.40)
2.0	5.71(0.58)	5.58(0.73)	6.38(0.17)
2.5	6.21(0.89)	6.10(0.67)	6.66(0.33)

* Values in parentheses are standard deviation.

Tests show that NOS had a significant effect on Young's modulus of the composite poles ($p = 0.0002$). The average MOE values were 5.3, 5.6, and 7.4 MPa for NOS of 6, 9, and 12. The 12-sided MOE was significantly higher than that of 6- or 9-

sided. The higher MOE of the 12-sided MOE may result from the effects of the glue-lines. There are 12 glue-lines one each of the 12-sided poles. The stiffness of the glue-line is higher that that of solid wood and allowed the composite pole to have higher MOE values.

Table 2.8 lists the Young's modulus values of full-size composite poles. When comparing these MOE values with those in Tables 2.6 and 2.7, it is noted that the stiffness of full-size composite poles was much higher than that of small-scale composite poles or solid poles. Full-size and small-scale composite poles basically belong to the same materials and would have the same stiffness. The addition of disks and fillings in the hollow part of the clamp side may change the properties of the full-size composite poles. In other words, the fillings below the ground-line may enhance the bending stiffness of the poles. Statistic analysis results show that strip thickness ($p = 0.3087$) and number ($p = 0.7529$) were not correlated to the MOE. The average MOE values were 10.8, 12.1, and 12.5 TPa for strip thickness of 1.91, 2.86, and 3.81 cm; and the average for 9 and 12 NOS were 11.6 and 11.9 TPa. There were no significant differences among different strip thickness levels and among different NOS levels.

Table 2.8. Modulus of elasticity of full-sized laminated composite poles.

Strip thickness (cm)	Modulus of elasticity (10^9Pa)	
	9-strip poles	12-strip poles
1.91	10.61(0.277)*	10.90 (2.578)
2.86	12.28(3.426)	12.84 (2.494)
3.81	12.04 (0.502)	12.92 (1.232)

* Values in parentheses are standard deviation.

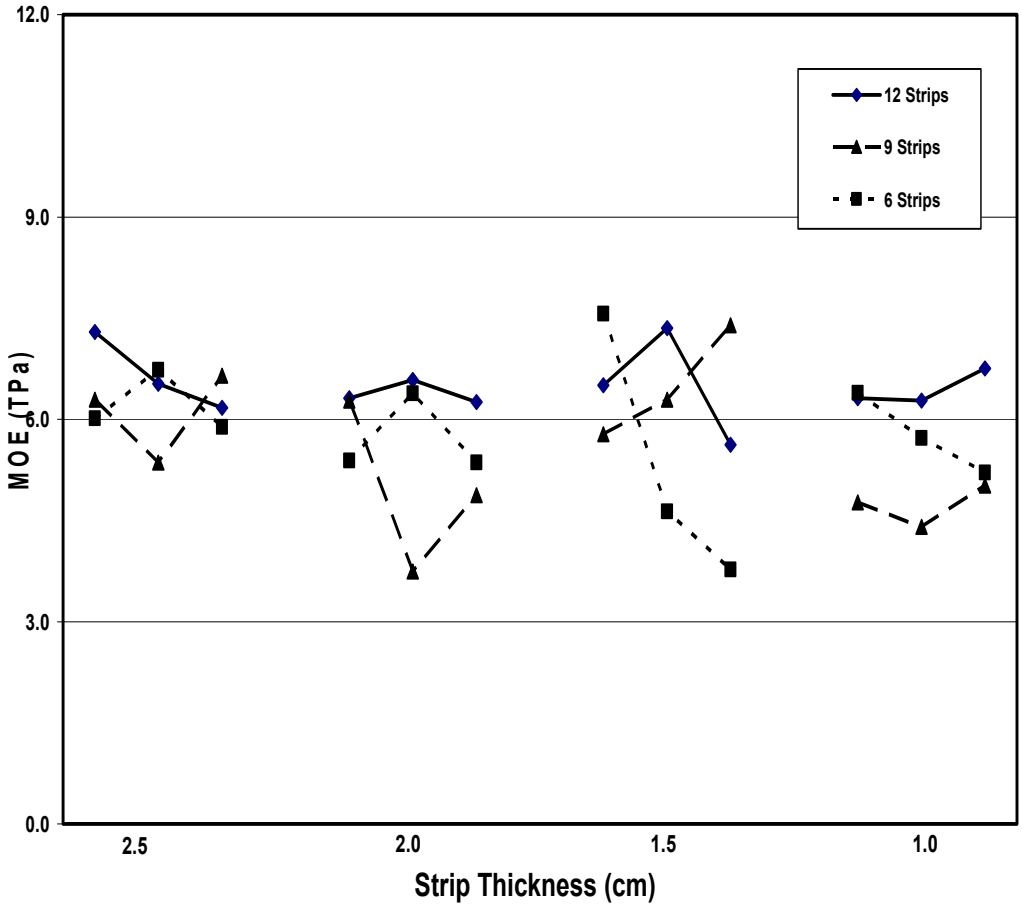

Figure 2.9 Effects of strip thickness and number on the modulus of elasticity of small-scale wood laminated composite poles.

2.5.3 Glue-Line Shear

The shear strength and wood failure in both dry and wet conditions in the glue-line shear test of small-scale composite poles are listed in Tables 2.9 and 2.10. In general, shear strength in the dry condition decreased with an increase of strip thickness. One of the exceptions is the 12-strip poles with 1.5 cm thick strip, the shear strength of which was much higher than the other groups. The percentage of wood failure of this group is lower than others in the same thickness level (Table 2.10). Statistic analysis shows that strip thickness effects were significant on shear strength and wood failure in both wet and dry conditions. In the dry condition, average shear strength values were 9.54, 8.80, 7.98, and 7.56 MPa for thickness levels of 1.0, 1.5, 2.0, and 2.5 cm, respectively; and the corresponding wood failure values were 50, 63, 69, and 72 percent for the four thickness levels, respectively. Figure 2.10 shows the effects of variables on samples' shear strength and Figure 2.11 gives the effects of variables on wood failure in the dry condition.

Table 2.9. Glue-line shear strength values before and after water soaking of small-scale composite poles.

Strip thickness	Shear in dry condition (MPa)			Shear in wet condition (Mpa)		
	6-strip	9-strip	12-strip	6-strip	9-strip	12-strip
2.5	7.33 (0.33)*	8.15 (1.15)	6.30 (1.08)	5.13(0.14)	5.36(0.33)	4.85(1.05)
2.0	5.96 (0.54)	7.68 (0.49)	10.29 (2.08)	4.61(0.26)	5.20(0.20)	4.81(0.26)
1.5	7.84 (0.88)	9.71 (0.03)	8.85 (1.45)	5.58(0.22)	5.34(0.69)	4.96(0.99)
1.0	10.08 (0.79)	10.15 (0.63)	8.39 (1.05)	7.01(1.84)	4.97(0.31)	5.33(0.20)

* Values in parentheses are standard deviation.

The greater shear strength of poles with thinner strips may be due to the fact that thinner shells received more pressure than the ones with thicker shells. During the making of the poles, the same force was added to the same molds. The thinner strips may

have greater pressure in the glue-line and have better bonding conditions because of their lower contact area between them. This indicates that sufficient pressure is necessary when making composite poles. Excessive pressure may cause the problem of squeezing glue out of the glue-line and lowering the bonding strength but that was not the case in this study. Among the four thickness levels, LSD results showed that the shear strength of each level was significantly different from the others, meaning that shear strength increased with the decrease of strip thickness i.e., increase of pressure.

Table 2.10 Percentage of wood failure in the glue-line shear test of wood composite poles.

Strip thickness	Shear in dry condition (%)			Shear in wet condition (%)		
	6-strip	9-strip	12-strip	6-strip	9-strip	12-strip
2.5	73.81 (7.30)*	68.75(12.37)	72.00 (7.17)	67.17 (6.76)	70.83(15.28)	46.67(13.33)
2.0	72.81(14.35)	75.92 (7.30)	57.72(12.80)	72.28(18.51)	54.89 (8.60)	44.92(13.81)
1.5	63.61(10.21)	70.22 (5.01)	54.50 (8.01)	47.50(12.50)	24.03(13.18)	46.25 (8.33)
1.0	52.92(35.22)	54.06 (9.67)	54.42 (3.88)	48.42(24.12)	38.75 (5.73)	35.14 (4.57)

* Values in parentheses are standard deviation.

Figures 2.10 and 2.11 show that shear strength increased and wood failure decreased as strip thickness decreased. It can be seen that high shear strength between thin strips corresponded with low wood failure and low shear strength between thick strips with high wood failure.

After the 2-hour boiling test, the shear strength was reduced to 5.11, 4.84, 5.30, and 5.77 MPa, and the wood failure was reduced to 41, 39, 55, and 62 percent for the four thickness levels, respectively. The poles with strip thickness from 1 to 2.5 cm lost 46, 45, 34, and 24 percent of the original strength, respectively. Thinner poles lost more strength after the treatment. In the wet condition, the poles with 2.5 cm strip thickness had the

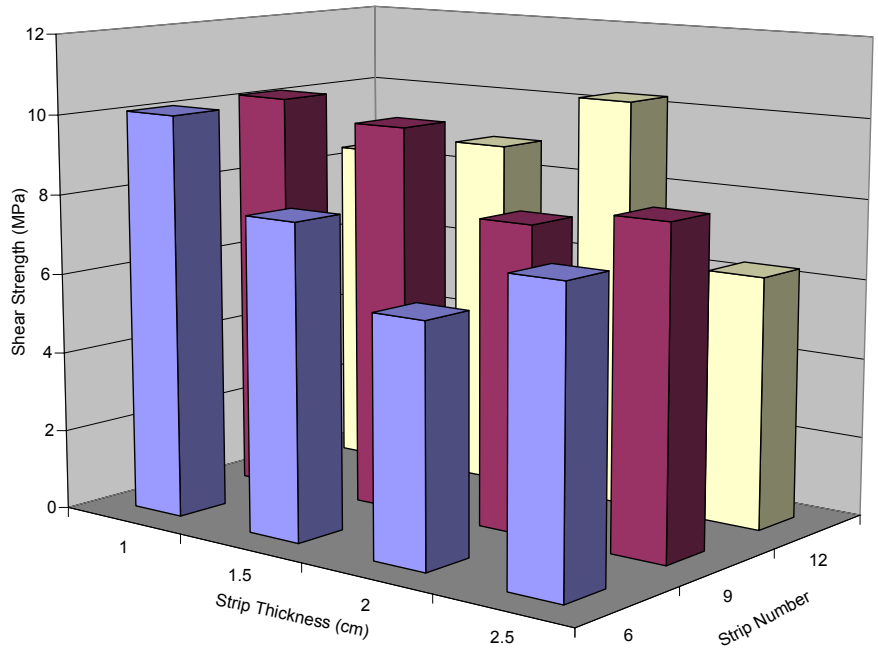

Figure 2.10. Effects of strip thickness and NUMBER OF STRIPS on the glue-line shear strength of wood composite poles.

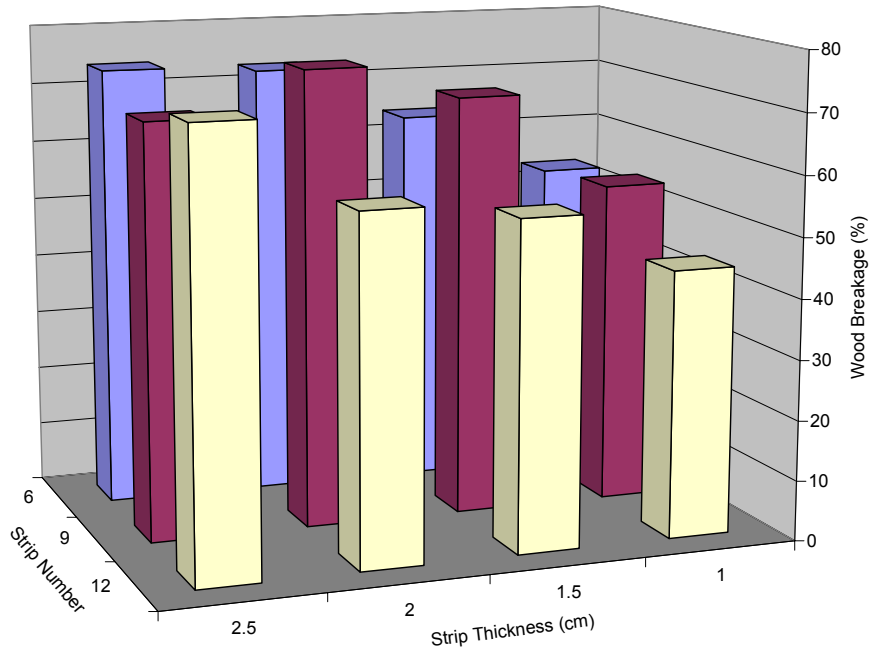

Figure 2.11. Effects of strip thickness and NUMBER OF STRIPS on wood failure in the glue-line shear test of wood composite poles.

highest shear value and was significant different from the others. There were no differences for the shear strength between the poles with thickness values of 2.0 and 1.0 cm, but both were higher than the ones at 1.5 cm thickness. Poles with thick strips still had higher wood failure, indicating they are more durable than poles with thin strips. Figures 2.12 and 2.13 show these trends.

Another factor that affects the shear strength and wood failure is the grain direction of the strips that form the glue-line. For the species used in this study, southern pine, earlywood and latewood alternatively appear on the cross section. The best scheme for the glue bond consideration is that the grain planes on both surfaces are parallel to the glue-line plane. Under this condition, the materials on the two bonding surfaces are uniform and good bonding quality may be obtained. In this case, the tangential direction of a wood strip coincides with the radial direction of the pole and the radial direction of a wood piece becomes tangential in the pole. Another advantage of this arrangement is that the tangential shrinkage of the pole will be minimized due to less shrinkage and swelling in the radial direction of the wood. The worst case for the glue bond is when the annual rings on both sides of the glue-line are perpendicular to the glue-line. The hardness of latewood is greater than that of the earlywood. If two latewood rings match up in the glue-line, they will affect the bonding of the earlywood rings next to the latewood rings. Also the tangential direction of the wood strips coincides with that of the pole, more shrinkage and swelling in the pole is expected. The effects of wood growth ring direction and the gluability of earlywood and latewood had great effects on the physical and mechanical properties of composite poles and will be further studied in the future.

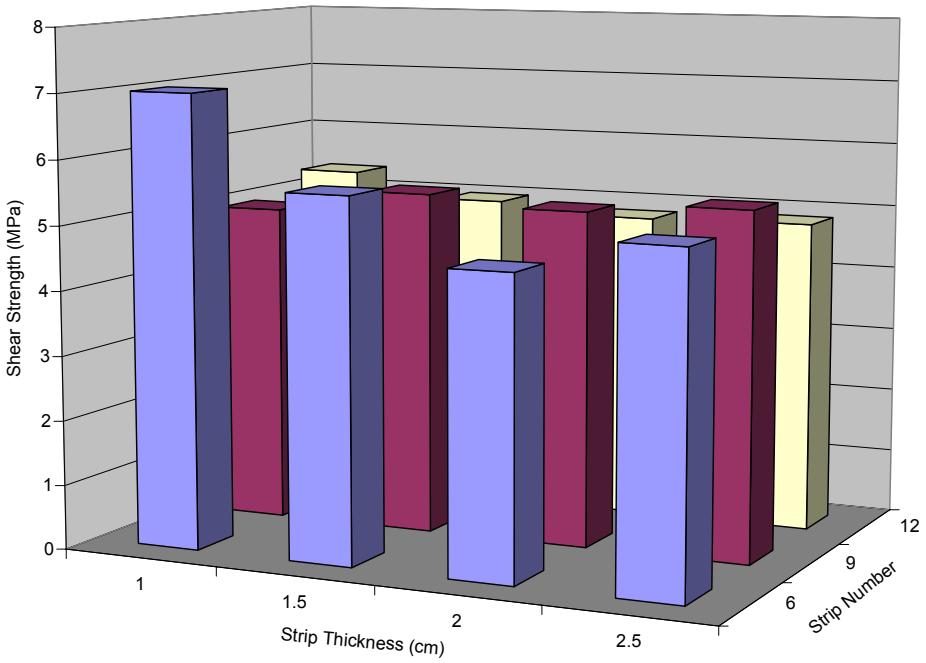

Figure 2.12. Effects of NUMBER OF STRIPS and thickness on the shear strength of wood composite pole samples after a 2-hour boiling test.

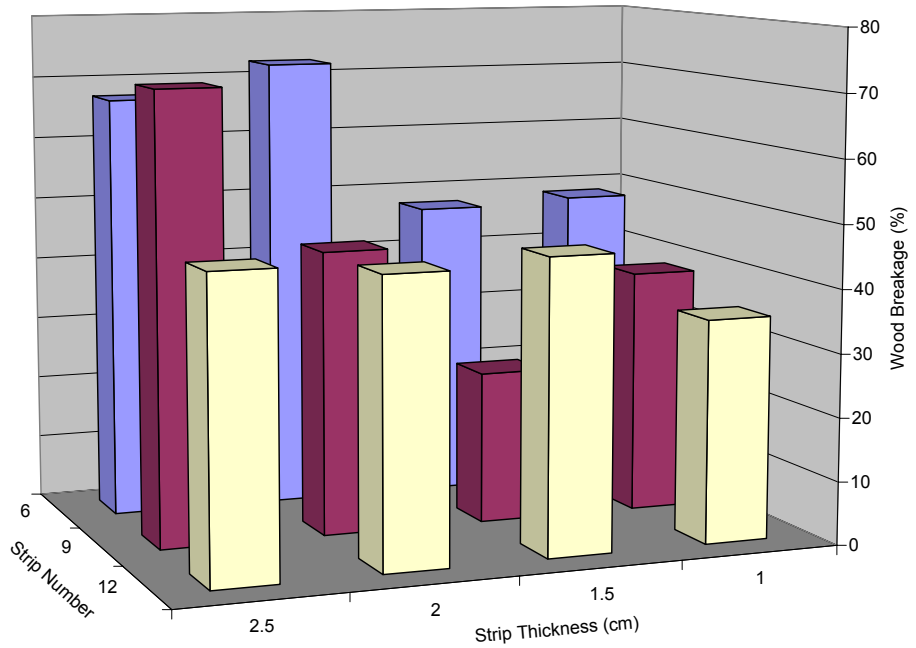

Figure 2.13. Effects of strip thickness and number on the wood failure of composite poles in the shear test after a 2-hour boiling treatment.

2.6 Conclusions

Full- and small-scale wood composite poles were fabricated, tested and analyzed. Small-scale poles were tested to failure and the glue-line shear strength in both wet and dry conditions were obtained from the unchanged properties of previously tested poles. The full-size poles were not tested to failure due to the need for subsequent experiment on these poles. Strain gages were attached to the full-size poles to obtain the strain during the test. Spruce and southern yellow pine solid poles were also processed and tested as controls for the analysis of composite poles. Strip thickness and NOS were the factors that affected the mechanical properties of composite poles:

1. Strip thickness had negative effects on the glue-line shear stress in both dry and wet conditions. Strip thickness was not correlated with the shear stress at the clamped end of the small-scale composite poles, the maximum bending stress of the small-scale composite poles, and Young's modulus of both full- and small-scale composite poles.
2. NOS is another important factor in determining the mechanical properties of composite poles. With an increase of NOS, the modulus of elasticity increased. It had no effects on the glue-line shear strength properties. More strips in a pole incurred more processing errors and resulted in poor bonding quality and pole integrity.
3. The "Two-hour heating + Two-hour boiling" treatment resulted in a reduction in shear strength and an increase in glue-line failure. Thinner strips lost more shear strength after the treatment and had low durability.

4. The modulus of elasticity of small-scale wood composite poles was inferior to that of solid poles with the same species. The modulus of elasticity of full-size wood composite poles was superior to that of solid poles.

2.7 References

Adams, R.D., S. Mateer, G.P. Krueger, A.E. Lund, D.D. Nicholas. 1981. Composite wood utility poles. EL-1745 Research Project 796-1. Prepared for Electric Power Research Institite. 3412 Hillview Avenue, Palo Alto, California 94304.

American Society for Testing and Materials. 1996. Standard methods of static test of wood poles, D 1036-58(64).

Erickson, R.W. 1995. Hollow veneered pole. U.S. Patent. Number 5,438,812.

CHAPTER 3

THEORETICAL MODELS OF LAMINATED WOOD COMPOSITE POLES

3.1 Introduction

In the analysis of bending beams, the classical Bernoulli-Euler theory has long been used as a convenient approximation for slender beams in structural analysis and design (Rehfield and Murthy 1982). The main assumption in this theory is that the transverse plane that is normal to the beam middle plane remains normal during bending. This assumption implies that the transverse shear strain and deformation are neglected. The Bernoulli-Euler theory may lead to serious discrepancies in cases of deep beams with small slender ratios (L/h) (Kant and Gupta 1988). The refinement of this theory has been attracting attention for almost one and a half of century (Kathnelson 1996). Among these efforts, Timoshenko (1921) improved the validity of the theory by incorporating the effect of transverse shear into the governing equations. This theory assumed that cross section remains a plane after bending and the shear stress is uniform through the thickness of the beam. In order to recognize the nonuniform shear stress distribution at a section, a factor is introduced into the shear stress formula. After this improvement, the classical theory can be used to calculate the deflection for short as well as long beams.

One of the earliest studies of shear effects on wood was done by Biblis (1965). Two methods were used in his study, i.e., an elementary direct method and the energy method. In the direct method, it was assumed that all cross sections were free to deform and the curve due to shear was represented by two straight lines, whereas the energy method has no such assumptions and is thus more accurate. His study shows that the

percentage of deflection due to shear is dependent on the span-to-depth ratios and could be as high as more than 50 percent when the ratio is 8:1.

Wood laminated composite poles are thick-wall beams with a polygonal cross section. The hollow beams have sufficient strength and stiffness properties but relatively low weight, as compared to solid wood poles. The merits that wood composite poles have, such as produced from renewable natural resources, broad material and material size requirements, and easy treatment make this hollow beam superior to poles and beams from other materials as well as solid wood poles. In addition to the applicability for utility poles, hollow wood composite beams may find applications in pillar, post, and engineering beams. To enhance the material and structural efficiencies, theoretical research is needed. The present study is to construct theoretical models through two methods (high-order differential equation, Timoshenko beam theory) to assess the stress and strain properties of this new engineered wood product. The high-order differential equation method was based on the energy method, i.e. the principle of minimum potential energy of wood composite poles. This general approach has been used in other literatures in solving beams and plates in bending. It is formulated in terms of scalar quantities such as work and energy. An advantage of energy methods is that they avoid some extraneous detail, such as geometric manipulation of deflection components. Another advantage is their ability to yield approximate solutions for problems too complicated to be solved exactly. The objective of this part of the study was to develop a theoretical model using high-order differential equations and the principle of minimum potential energy to assess and predict the properties of wood composite poles.

3.2 High-Order Differential Equations

The target composite pole of this study is composed of a number of wood strips bonded with an adhesive. The thickness of the strips are less than the radius of the circle outside the cross section, thus the poles are hollow inside. Figure 3.1 shows a typical design of a polygonal wood composite pole and its right-hand set of coordinate axes *x*, *y*, and *z*. The corresponding axial displacements are *u*, *v*, and *w*. The NOS in one pole is 3n, where n is 1, 2, 3, etc. The pole shown in the Figure 3.1 is one of the target poles analyzed in this study. It has 12 strips and 12 glue lines.

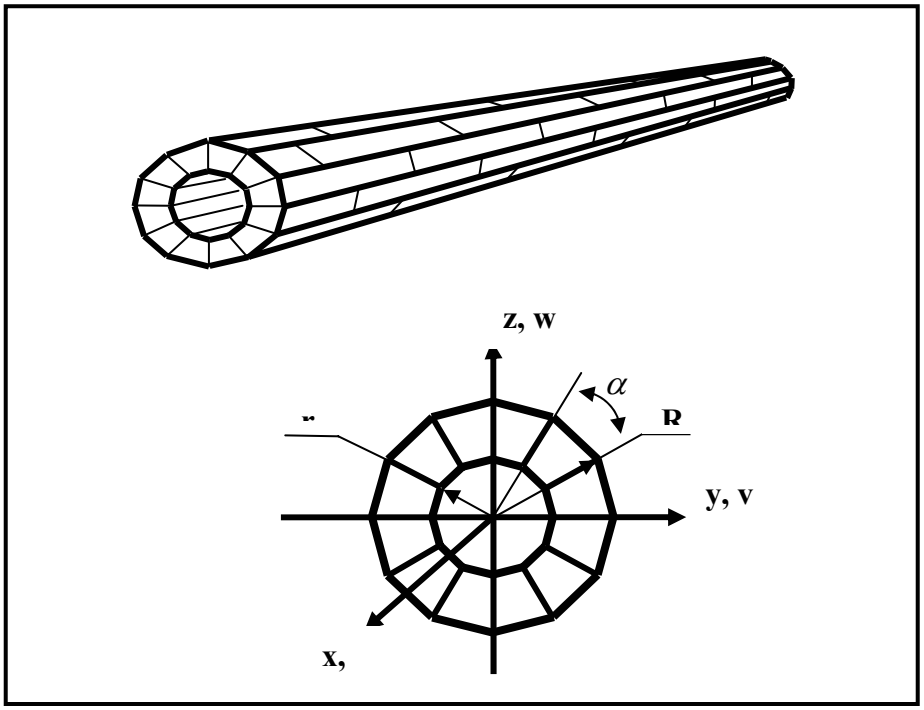

Figure 3.1. A schematic diagram of a wood composite pole and its coordinates.

The lateral displacement (*w*) of the pole was assumed to consist of four parts: the elementary theories of normal and shear displacements of the wood strips and glue layers. In this section, the normal and shear strain energies for wood and glue layers were

derived. Since the thickness of each glue layer is much thinner than that of a wood strip, the glue layer thickness was neglected in the analysis of strain energy of wood strips. The strain energy stored in glue layers was analyzed separately from wood strips.

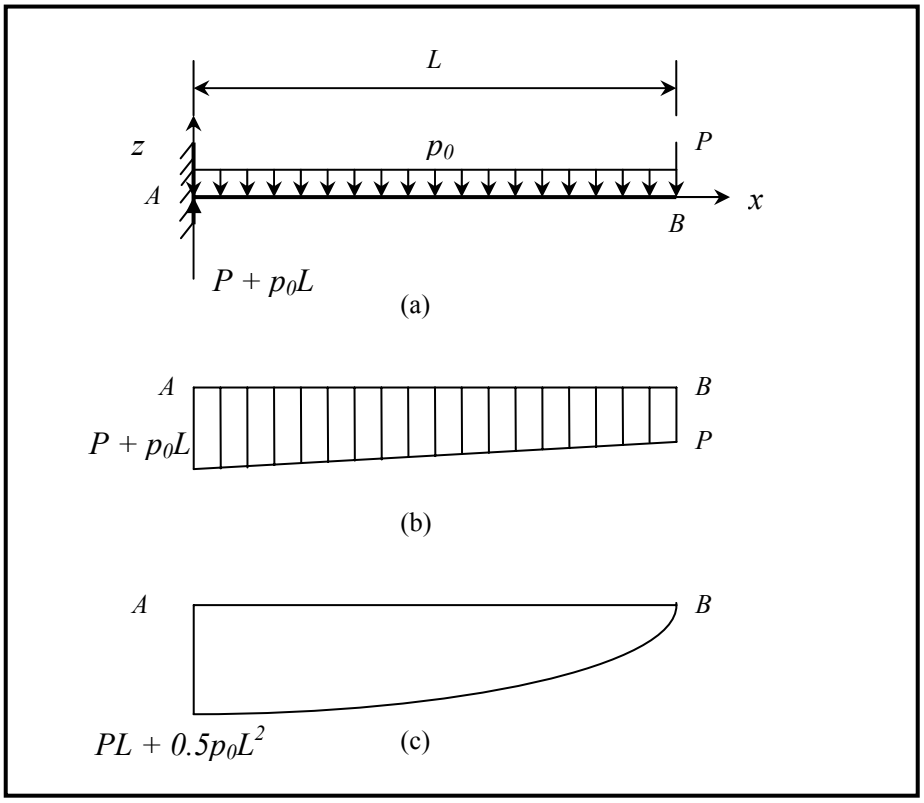

Figure 3.2. A loading system and shear and moment distribution of a cantilever beam.

According to the theories, the normal and shear stresses of the pole can be expressed as

$$\sigma_x = \frac{Mz}{I} \tag{3.1}$$

$$\tau_{xy} = \frac{dM}{dx}\frac{1}{bI}\int_z^R zdA = \frac{VQ}{Ib} \tag{3.2}$$

where M is the bending moment, I is the moment of inertia of the cross section of the pole, V is the vertical shear force, b is the width of the pole, and Q is the first moment. The strain energy density function for a beam, in Cartesian coordinate system, is defined as

$$W_\sigma = \frac{1}{2}\sigma_x \varepsilon_x \tag{3.3}$$

$$W_\tau = \frac{1}{2}\tau_{xy}\gamma_{xy} \tag{3.4}$$

where

$$\varepsilon_x = \frac{du_x}{dx} = -z\frac{d^2w}{dx^2} \tag{3.5}$$

$$\gamma_{xy} = \frac{\tau_{xy}}{G} \tag{3.6}$$

Thus, the strain energy functions becomes

$$W_\sigma = \frac{1}{2}\sigma_x\varepsilon_x = \frac{1}{2}E\varepsilon_x^2 = \frac{1}{2}E(\frac{d^2w}{dx^2})^2 z^2 \tag{3.7}$$

$$W_\tau = \frac{1}{2}\tau_{xy}\gamma_{xy} = \frac{1}{2}\frac{\tau_{xy}^2}{G} = \frac{1}{2}\frac{V^2Q^2}{GI^2b^2} \tag{3.8}$$

Since $V = -EI\frac{d^3w}{dx^3}$ (elementary mechanics), Equation 8 becomes

$$W_\tau = \frac{1}{2}\frac{V^2Q^2}{GI^2b^2} = \frac{1}{2}\frac{E^2Q^2}{Gb^2}(\frac{d^3w}{dx^3})^2. \tag{3.9}$$

After integrating Equations 7 and 9 with respect to y and z and substituting the value of *I*, we have the normal strain energy and shear strain energy stored in the pole as the followings:

$$U_\sigma = \frac{EI}{2}\int_0^L (\frac{d^2w}{dx^2})^2 dx \tag{3.10}$$

$$U_\tau = \frac{E^2}{2G}\int_0^L (\frac{d^3w}{dx^3})^2 dx \int_A \frac{Q^2}{b^2} dydz \tag{3.11}$$

Thus we obtained the general expressions of the strain energies for both the wood and glue layers. Let $k_1 = \int_A \frac{Q^2}{b^2} dydz$, then shear strain energy for the whole pole has the form

$$U_\tau = \frac{k_1 E^2}{2G}\int_0^L (\frac{d^3w}{dx^3})^2 dx \tag{3.12}$$

In the design of this study, the pole has 3n strips, and thus 3n glue layers. Take the 12-strip pole as an example, the pole has 12 strips and glue layers, as shown in Figure 3.3. The strain energy of each glue layer is the sum of strain energy caused by normal and shear strain. And the total strain energy of the glue layers is the sum of the strain energy for each glue layer:

$$\begin{aligned} U_g &= U_{\sigma-AA'} + U_{\tau-AA'} + U_{\sigma-BB'} + U_{\tau-BB'} + \cdots + U_{\sigma-LL'} + U_{\tau-LL'} \\ &= U_{AA'} + U_{BB'} + \cdots + U_{LL'}. \end{aligned}$$

Since some of them are equal, the total strain energy of the glue layers can be expressed as

$$\begin{aligned} U_g &= 2U_{AA'} + 4U_{BB'} + 4U_{CC'} + 2U_{DD'} \\ &= k_6\int_0^L (\frac{d^2w}{dx^2})^2 dx + k_7\int_0^L (\frac{d^3w}{dx^3})^2 dx \end{aligned} \tag{3.13}$$

where

$$k_6 = E_g(I_{g1} + 2I_{g2} + 2I_{g3})$$

$$k_7 = k_5(k_1 + k_2 + k_3 + k_4)$$

$$k_5 = \frac{E_g^2}{2G_g}$$

$$k_4 = 2\iint_A \frac{Q_{g1}^2}{t^2 I_{g1}} dA$$

$$k_3 = 4\iint_A \frac{Q_{g2}^2}{t^2 I_{g2}} dA$$

$$k_2 = 4\iint_A \frac{Q_{g3}^2}{t^2 I_{g3}} dA$$

$$k_1 = 2\iint_A \frac{Q_{g4}^2}{t^2 I_{g4}} dA$$

and I_{g1}, I_{g2}, and I_{g3} are the moment of inertia of glue layers, Q_{g1}, Q_{g2}, Q_{g3}, and Q_{g4} are the first moment of each of the glue lines, E_g is the Young's modulus of glue, G_g is the rigidity of glue, and A is the area of the cross section.

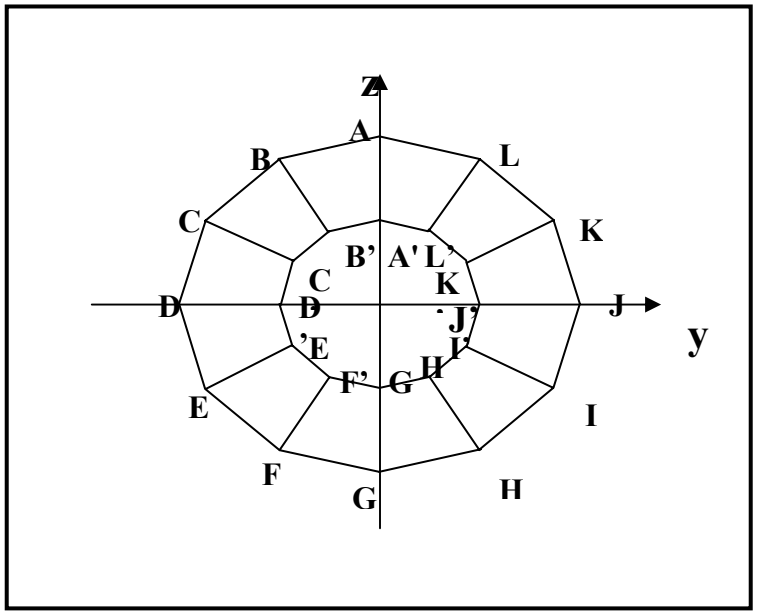

Figure 3.3. A schematic diagram of the cross section of a 12-strip pole shell.

Two external forces are applied to the pole system. They are body force of pole (p_0) and the applied concentrated load (P) at the free end. Then the work done by the external force is as followings

$$H = -\int_0^L p_0 w dx - Pw(L) \tag{3.14}$$

where

H - work done by the external force

p_0 - body force of the pole

w - transverse displacement along the length of the pole L

The total potential energy is given as

$$\pi = U_\sigma + U_\tau + U_g + H \tag{3.15}$$

Substitute Equations 10, 12, 13, and 14 into Equation 15 and rearrange, the total potential energy is given by

$$\pi = k_8 \int_0^L \left(\frac{d^2 w}{dx^2}\right)^2 dx + k_9 \int_0^L \left(\frac{d^3 w}{dx^3}\right)^2 dx - \int_0^L p_0 w dx - Pw(L) \tag{3.16}$$

where

$$k_8 = \frac{1}{2} EI + k_6$$

$$k_9 = \frac{k_1 E^2}{2G} + k_7$$

The principle of minimum potential energy states that "of all the displacements which satisfy the boundary conditions of a structural system, those corresponding to stable equilibrium configurations make the total potential energy a relative minimum." According to this principle, the system is in equilibrium when the first variation in π vanishes. Thus the equilibrium condition is

$$\delta\pi = \frac{\partial\pi}{\partial x}dx = 0$$

or

$$k_8\int_0^L 2\frac{d^2w}{dx^2}\delta(\frac{d^2w}{dx^2})dx + k_9\int_0^L 2\frac{d^3w}{dx^3}\delta(\frac{d^3w}{dx^3})dx - \int_0^L p_0\delta w dx - P\delta w(L) = 0 \quad (3.17)$$

Equation 17 yields one differential equation, which is the governing differential equation for the pole loading system.

$$k_9\frac{d^6w}{dx^6} + k_8\frac{d^4w}{dx^4} - \frac{p_0}{2} = 0 \quad (3.18)$$

with boundary conditions

$$[k_9\frac{d^5w}{dx^5} - k_8\frac{d^3w}{dx^3})]_{x=L} = \frac{P}{2} \quad (3.19)$$

$$(k_8\frac{d^2w}{dx^2} - k_9\frac{d^4w}{dx^4})|_{x=L} = 0 \quad (3.20)$$

$$k_8\frac{d^3w}{dx^3}|_{x=0} = 0 \quad (3.21)$$

The other boundary conditions may be as followings

$$w|_{x=0} = 0 \quad (3.22)$$

$$w'|_{x=0} = 0 \quad (3.23)$$

$$k_8\frac{d^2w}{dx^2}|_{x=L} = 0 \quad (3.24)$$

Then the following solution is obtained

$$w = c_1 + c_2x + c_3x^2 + c_4x^3 + \frac{1}{48k_8}p_0x^4 + c_5e^{k_{10}x} + c_6e^{-k_{10}x} \quad (3.25)$$

where

$$k_{10} = \sqrt{\frac{k_8}{k_9}}$$

and c_1 to c_6 are constants and given as follows:

$$C_1 = \frac{k_{10}(p_0 L + P)(e^{k_{10}L} - e^{-k_{10}L}) + 2p_0}{2k_8 k_{10}^4 (e^{k_{10}L} + e^{-k_{10}L})}$$

$$C_2 = -\frac{p_0 L + P}{2k_8 k_{10}^2}$$

$$C_3 = \frac{p_0 L^2 + 2PL}{8k_8} + \frac{p_0}{2k_8 k_{10}^2}$$

$$C_4 = -\frac{p_0 L + P}{12k_8}$$

$$C_5 = \frac{k_{10}(p_0 L + P)e^{-k_{15}L} - p_0}{2k_8 k_{10}^4 (e^{k_{10}L} + e^{-k_{10}L})}$$

$$C_6 = -\frac{k_{10}(p_0 L + P)e^{-k_{15}L} + p_0}{2k_8 k_{10}^4 (e^{k_{10}L} + e^{-k_{10}L})}$$

3.3 Solutions Based on Timoshenko Beam Theory

U, *V*, and *W* are the displacement at x, y, z directions, respectively. Since *U* is a function of (x, y, z), we expand U into a Tylor series (Washizu 1968, Kant and Gupta 1988) about z = 0:

$$U(x, y, z) = U(x, y, 0) + \left(\frac{\partial U}{\partial z}\right)_{z=0} z + \frac{1}{2!}\left(\frac{\partial^2 U}{\partial z^2}\right)_{z=0} z^2 + \ldots \tag{3.26}$$

After retaining the first two terms of Equation 26,

$$\vec{U} = \vec{U}_0 + z\vec{U}_1 \tag{3.27}$$

where $\vec{U}_1 = u_1\vec{i}_1 + w_1\vec{i}_3$. Equation 27 is an expression that includes the effect of transverse shear deformation. Two assumptions were made: (1) a cross section perpendicular to undeformed central line remains perpendicular to the deformed locus; (2) the displacement is small. Then we have

$$U = u + z\,u_1,\ V = 0,\ W = w$$

$$\varepsilon_x = \mathbf{u}' + \mathbf{z}\,\mathbf{u}_1',\ \gamma_{xz} = \mathbf{w}' + \mathbf{u}_1 \tag{3.28}$$

The total strain energy of the beam may be expressed as

$$\pi = \iiint_{C} (\sigma_x \varepsilon_x + \tau_{xz}\gamma_{xz})dxdy\mathbf{dz} - \int_0^L p_0 w dx - Pw \tag{3.29}$$

According to principle of minimum potential energy, the system is in equilibrium when the first variation in π vanishes:

$$\delta\pi = \iiint_{V} (\sigma_x \delta\varepsilon_x + \tau_{xz}\delta\gamma_{xz})dxdydz - \int_0^L p_0 \delta w dx - P\delta w = 0 \tag{3.30}$$

Substitute Equation 28 into Equation 30, we obtain the following equation

$$-\int_0^L [\, N\delta\mathbf{u}' + M\delta\mathbf{u}_1 + Q(\delta\mathbf{w}' + \delta\mathbf{u}_1) - p_0\delta\mathbf{w}]\mathbf{dx} - P\delta v = 0 \tag{3.31}$$

where

$$N = \iint_S \sigma_x\, dydz \quad , \quad M = \iint_S \sigma_x\, z dydz \quad ,$$

$$Q = \iint_S \tau_{xz}\, dydz \tag{3.32a, b, c}$$

N is the axial force, M the bending moment, and Q the shear force. Integrate Equation 31 and rearrange, the following Equation may be obtained

$$\int_0^L [N'\delta u + (Q - M')\delta u_1 + (Q' + p_0)\delta w]dx -$$

$$[N\delta u + (P - Q)\delta w + M\delta u_1]_{x=L} - [N\delta u + Q\delta w + M\delta u_1]_{x=0} = 0 \quad (3.33)$$

Then the governing differential equations are as followings:

$$Q' = p_0 \quad (3.34a)$$

$$M' = Q \quad (3.34b)$$

$$N' = 0 \quad (3.34c)$$

and boundary conditions $P = Q|_{x=L}$, also

$$\mathbf{u(0) = w(0) = u_1(0)|_{x=0} = 0}$$

$$M|_{x=L} = 0$$

Based on these boundary conditions, Equation 34 may be solved. Substitute Equation 28 into Equation 32, we have

$$N = \iint_S \sigma_x dydz = E\iint_S (u' + zu_1')dydz = EAu'$$

$$M = \iint_S \sigma_x z dydz = E\iint_S \varepsilon_x z^2 dydz = EIu_1'$$

$$Q = \iint_S \tau_{xz} dydz = E\iint_S G\gamma_{xz} dydz = Gk(w' + u_1) \quad (3.35a, b, c)$$

where k is a Timoshenko constant and determined by the following formula (Shames and Dym 1985):

$$k = \frac{6(1+\nu)(1+m)^2}{(7+6\nu)(1+m) + (20+12\nu)m^2} \quad (3.36)$$

where $m = D/d$. D is the diameter of circumscribe circle of the cylinder, and d is the diameter of the inscribe cycle, v is the Piosson ratio. Substitute Equation 35 into Equation 34 and notice that no axial loads were added,

$$EIu_1'' = kGA\,(w' + u_1) \tag{3.37}$$

$$KGA[w' + u_1]' = -p_0 \tag{3.38}$$

Take derivative of Equation 37 and substitute Equation 38, we have

$$EIu_1''' = kGA(w'' + u_1') = p_0$$

Integrate the above equation three times, we have

$$EIu = -\frac{1}{6}p_0x^3 + \frac{1}{2}C_1x^2 + C_2x + C_3 \tag{3.39}$$

where C_1, C_2, C_3 are constants. Solve Equation 39 using boundary conditions, we obtain the deflection function of a cantilever beam subjected to body and concentrated loads:

$$w = \frac{p_0L^3}{24EI}x^4 - \frac{P + p_0L}{6EI}x^3 + \left(\frac{2PL + p_0L^2}{4EI} - \frac{p_0}{2kGA}\right)x^2 + \frac{P + p_0L}{kGA}x \tag{3.40}$$

and the maximum deflection is

$$w_{\max} = \frac{PL^3}{3EI} + \frac{p_0L^4}{8EI} + \frac{PL}{kGA} + \frac{p_0L^2}{2kGA} \tag{3.41}$$

It is noted that the first and second terms on the right side of Equation 41 are the bending parts of the total deflection caused by concentrated and body force loads, while the last two terms are the shear parts of the total deflection. It is also noted that the EI and GA in Equations 40 and 41 are the sum of both wood strips and glue layers so that the glue layer effects may be taken into account in the total deflection.

3.4 Experimental Study

To validate the applicability of the theoretical models and to predict the deflection, an experimental investigation was conducted on the reduced- and full-size composite poles. The experiment validation data was from Chapter 2. The species was southern yellow pine. Strip thickness and NOS are the two variables of the two kinds of composite poles. For the small-scale composite poles, strip thickness levels were 1.0 cm (0.4 in), 1.5 cm (0.6 in), 2.0 cm (0.8 in), and 2.5 cm (1.0 in), each of which had 6, 9, and 12 NOS. The length of the poles was 1.06 m (48 in). For the full-size poles, the strip thickness levels 1.9 cm (0.75 in), 2.9 cm (1.125 in), and 3.8 cm (1.5 in) and NOS was 9 and 12. Pole length was 5.16 m (20 ft.). There were three replications of each combination of strip thickness and number levels. Lumber was first planed to specific thickness and then cut to target size strips on a table saw. Commercially obtained resorcinol-phenol-formaldehyde (RPF) resin was used to bond the strips. The viscosity and specific gravity of RPF were 800 cps and 1.177. The glue was uniformly hand-spread onto the two lateral side surfaces at 310 g/m^2 (63.3lbs/1000 ft^2). Poles were pressed in molds for 36 hours in an air-conditioned room.

A cantilever test was performed for all the composite poles on a REVEL machine. Before the test, the control system of the REVEL was replaced by a digital controller and connected to a computer. The set-up of the test is shown in Figure 2.4. All small-scale composite poles were tested to failure to obtain the maximum bending stress. A load of 350 N (80 lbs) was added to each of the full-size composite poles to secure that the test was in the elastic range. Then the poles were taken off from the supporting frame and stored for future tests.

3.5 Results and Discussions

3.5.1 Results of Theoretical Study

The theoretical solution coefficients of the high-order differential equation are given in Table 3.1 for small-scale composite poles and Table 3.2 for full-size composite poles. All small-scale poles were visually loaded to 222 N (50 lbs) and full-size composite poles were visually loaded to 133 N (30 lbs). For both small- and full-size poles, the absolute values of the coefficients decreased with the increase of strip thickness. Since the thinner poles always have greater deflection under the same load level, there is a positive relation between the coefficients and the size and thickness of the composite poles. This may be seen through the comparison between Tables 3.1 and 3.2, i.e., the absolute values of coefficients of the full-size poles were normally larger than the absolute values of those of small-scale ones. The data shows little trends regarding the NOS effects on the coefficients for both sizes of composite poles.

Variation of deflection of small-scale composite poles with different NOS and thickness levels is plotted in Figure 3.4. The variation of deflection of full-size composite poles was plotted in Figure 3.5. It can be seen that the deflection increased as the decrease of strip thickness for both pole sizes.

Comparisons were made between the high-order differential equation model and the Timoshenko beam model. Figures 3.6 and 3.7 plot the results of variation of deflection for small- and full-size composite poles, respectively. Values from Timoshenko beam model and high-order differential equation models were close to each other.

Table 3.1. Coefficients of the deformation model of small-scale composite poles with three levels of number of strips and four levels of strip thickness.

Strip Number	Strip thickness (cm)	C_1 (10^{-4})	$\mathbf{C}_2$ (10^{-4})	C_3 (10^{-4})	C_4 (10^{-6})	C_5 (10^{-18})	C_6 (10^{-4})
12	1.0	3.46	-1.34	4.19	-3.33	2.77	-3.46
	1.5	2.57	-1.02	3.34	-2.65	0.94	-2.57
	2.0	2.16	-0.89	3.16	-2.51	0.21	-2.16
	2.5	2.21	-0.85	2.66	-2.11	1.87	-2.21
9	1.0	2.90	-1.32	5.81	-4.61	0.01	-2.90
	1.5	2.40	-1.03	3.99	-3.17	0.05	-2.40
	2.0	2.21	-0.92	3.40	-2.70	0.92	-2.21
	2.5	2.12	-0.89	3.29	-2.61	0.10	-2.12
6	1.0	3.46	-1.44	5.25	-4.16	0.23	-3.46
	1.5	2.83	-1.12	3.73	-2.96	0.91	-2.83
	2.0	2.14	-1.02	4.85	-3.85	0.00	-2.14
	2.5	2.23	-1.00	4.27	-3.39	0.01	-2.23

Model: $w = C_1 + C_2 z + C_3 z^2 + C_4 z^3 + \frac{1}{48k_1} P_0 z^4 + C_5 e^{k_2 z} + C_6 e^{-k_2 z}$

Table 3.2. Coefficients of the deformation model of full-size composite poles with two levels of number of strips and three levels of strip thickness.

Strip Number	Strip thickness (cm)	C1 (10^{-5})	C2 (10^{-5})	C3 (10^{-4})	C4 (10^{-7})	C5	C6 (10^{-5})
12	1.91	6.25	-1.75	1.40	-2.28	1.31×10^{-54}	-6.25
	2.86	4.07	-1.23	1.16	-1.87	2.83×10^{-59}	-4.07
	3.81	3.70	-1.14	1.10	-1.79	1.20×10^{-59}	-3.70
9	1.91	9.39	-2.45	1.71	-2.79	4.69×10^{-51}	-9.39
	2.86	3.55	-1.13	1.16	-1.89	2.06×10^{-61}	-3.55
	3.81	5.41	-1.58	1.37	-2.24	1.05×10^{-56}	-5.41

Model: $w = C_1 + C_2 z + C_3 z^2 + C_4 z^3 + \frac{1}{48k_1} P_0 z^4 + C_5 e^{k_2 z} + C_6 e^{-k_2 z}$

Shear effects on the deflection of small-scale poles were calculated by the Timoshenko beam model and plotted in Figure 3.8. Both strip thickness and number had effects on shear. Shear effects increased with the decrease of strip thickness and with an increase of NOS. The deflection due to shear accounted for from 0.8 to 1.9 percent of the total deflection for the small-scale composite poles and from 0.2 to 0.9 percent of the full-size composite poles.

Glue layer effects on the deflection of composite poles were analyzed. In the analysis, the thickness of the glue layer was set at 0.10 mm (0.004 in), and the Young's modulus and modulus of rigidity of cured resorcinol-phenol-formaldehyde resin were approximated as 38.6 and 2.1 TPa (5.6 and 0.31 Mpsi). The length, first and second moment, and normal and shear energies were calculated and included in the models. For the small-scale poles, the deflection that caused by glue layer was from 2.3 to 5.5 percent. The percentage for the full-size composite poles was from 4.13 to 6.89 percent. No regular pattern was found on the effects of strip thickness and number.

3.5.2 Comparison with Experimental Results

The maximum experimental deflection values under different loads were compared with the theoretical ones and are given in Tables 3.3 and 3.4. Table 3.3 lists the results from the small-scale composite poles, whereas Table 3.4 lists the results from the full-size composite poles. In both tables, each value is the average of three individual tested or predicted values because they were the replication samples of the combination of strip thickness and NOS variables. The high-order differential equation values are found to be smaller than the Timoshenko values for the small-scale composite poles; but for the full-size poles, the trends were inversed. The experimental values were greater

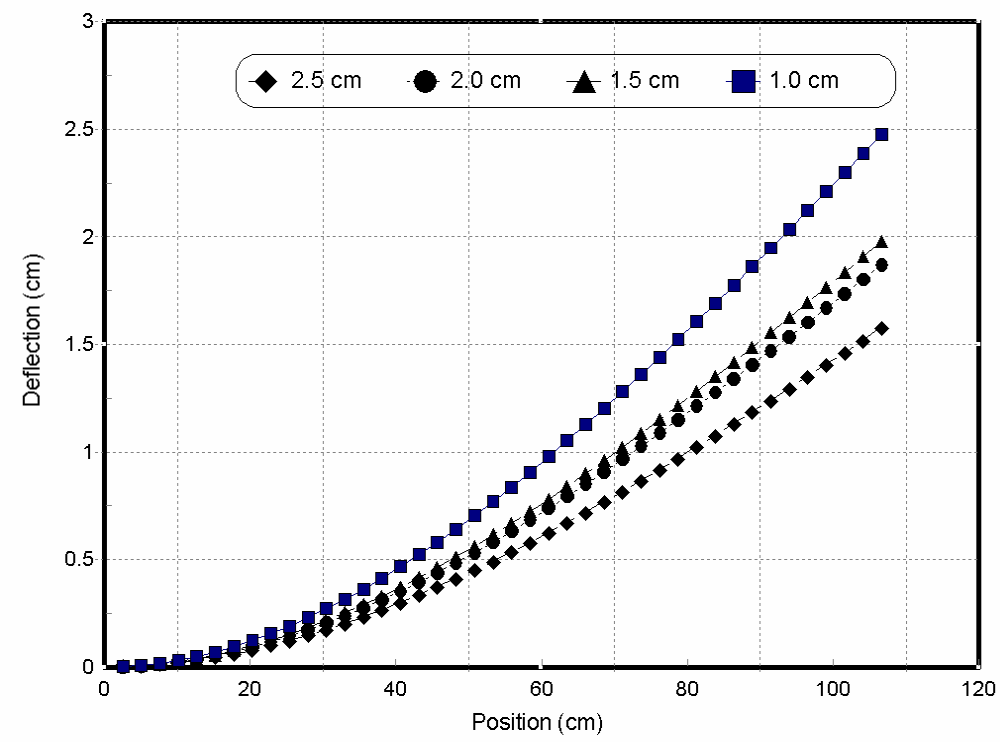

Figure 3.4. Deflection of 12-sided small-scale composite poles predicted by a high-order differential equation model.

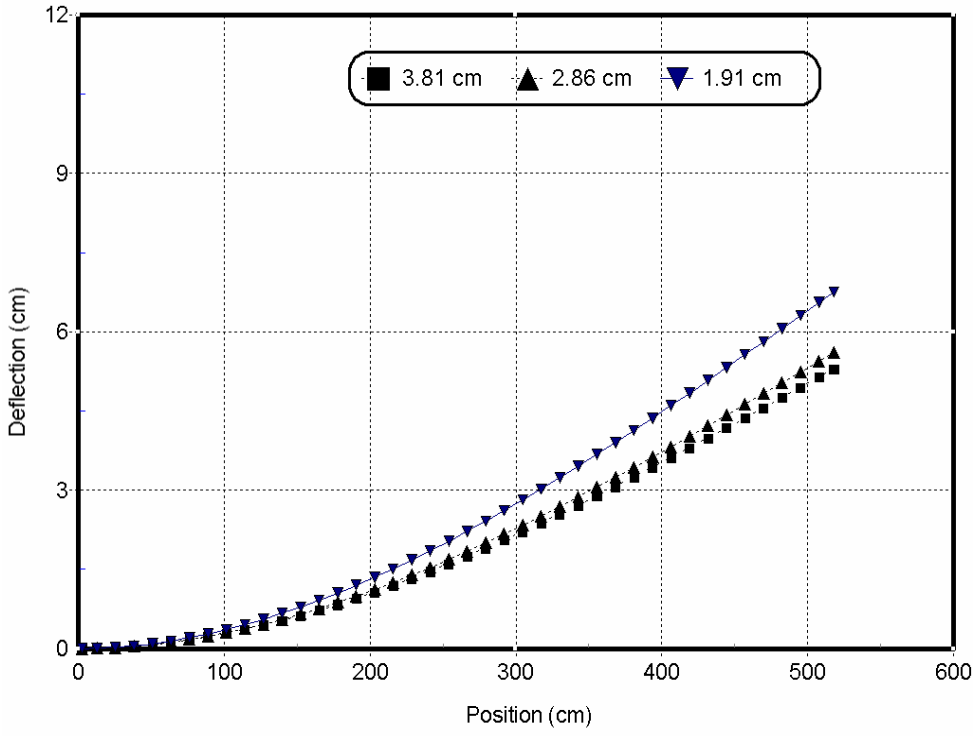

Figure 3.5. Deflection of 12-sided full-size composite poles predicted by a high-order differential equation model.

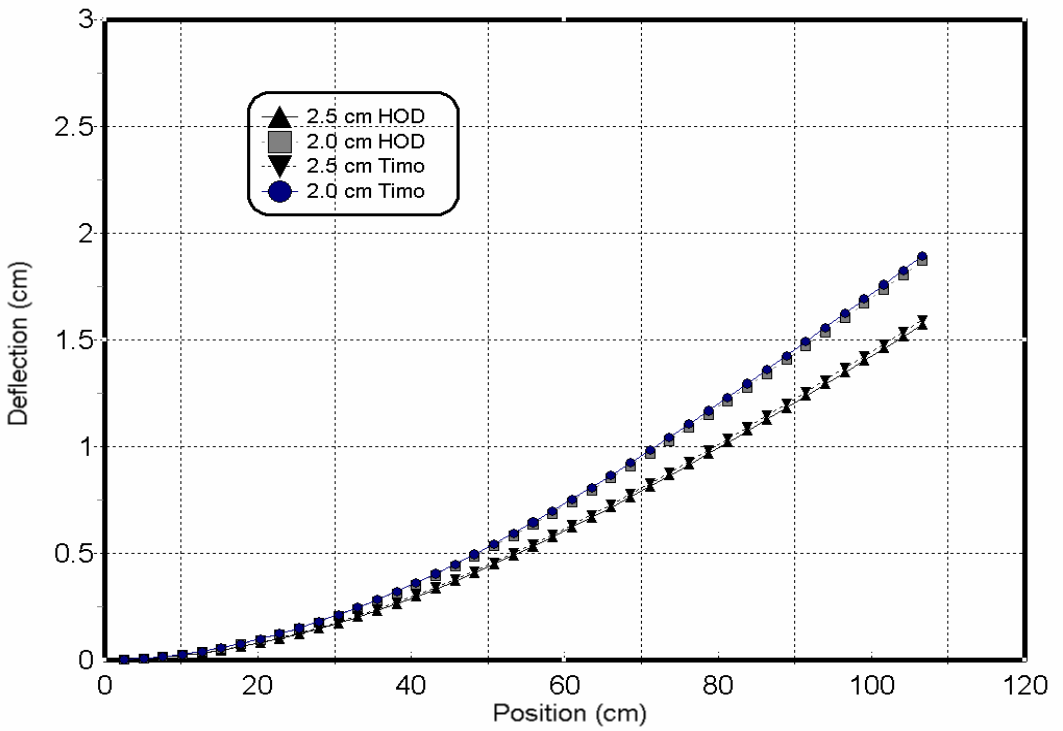

Figure 3.6. Comparison of deflection of 12-sided small-scale composite poles predicted by a high-order differential equation and Timoshenko beam models.

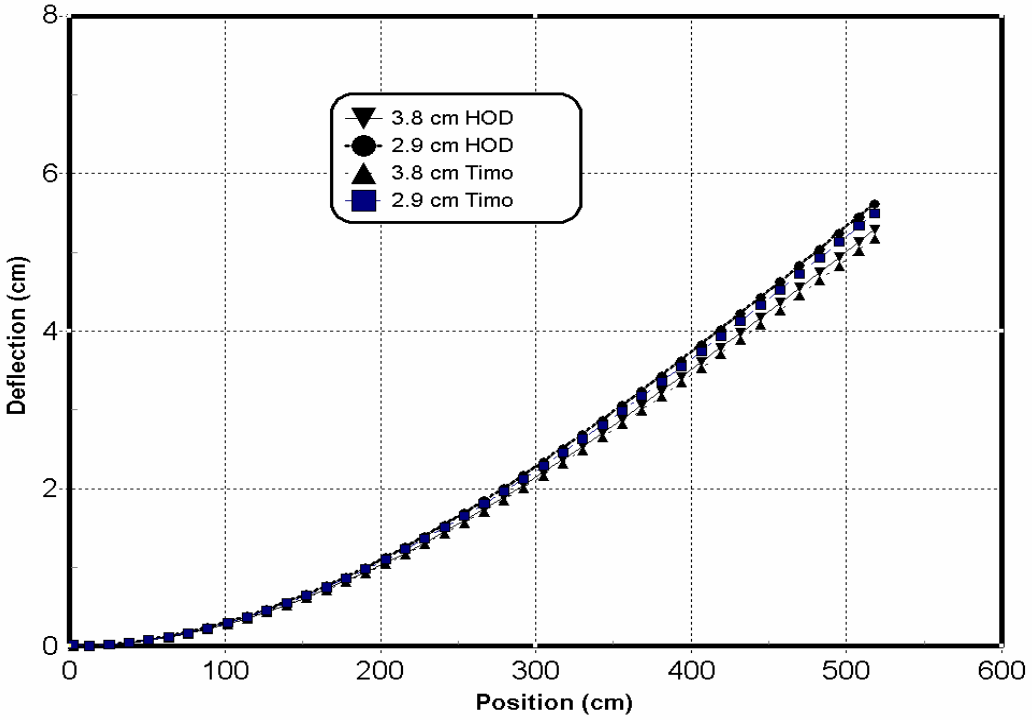

Figure 3.7. Deflection of 12-size full-size composite poles predicted by high-order differential equation and Timoshenko beam models.

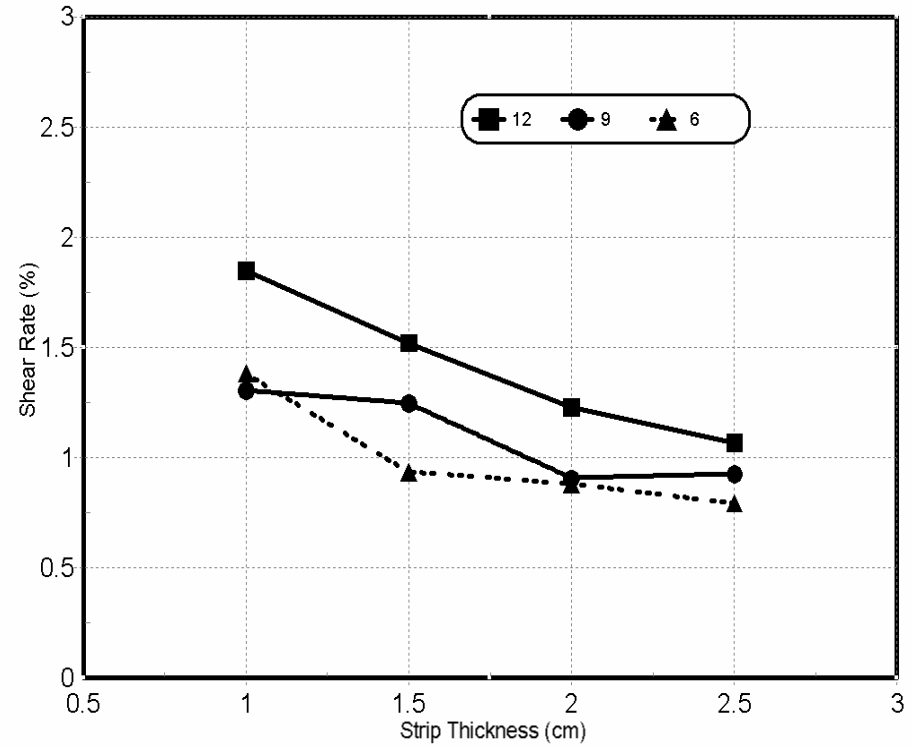

Figure 3.8. Effects of strip thickness and number of strips on the shear deflection of small-scale composite poles.

than both theoretical ones for the small-scale poles, but for the full-size poles, the experimental values varied between those from the theoretical ones. There were no regular patterns in the effects of strip thickness and NOS on the error rates of the two theoretical models for both small- and full-size poles.

Table 3.5 presents the maximum bending stress values obtained from experiment and from a theoretical model for the small-scale poles. The loads that were visually added in the model were the peak loads for each pole in the experimental test. Values from experiment and from the model were matched well.

Figure 3.9 shows the distribution of normal stress in the cross section. The normal stress reached the maximum on the top and bottom skins and zero on the central plane.

3.5.3 Discussions

High-order differential equation and Timoshenko beam models were validated by the experimental data. As shown in Tables 3.3 and 3.4, the error rates of the high-order differential equation ranged from 3.9 to 8.2 percent for the small-scale composite poles, and from 2.1 to 7.4 percent for the full-size composite poles, compared to the experimental values. In the analyses of small-scale composite poles, the error rates of the higher differential equation model mostly were higher than those of the Timoshenko beam model. The average error rates for the two models were 6.4 and 4.8 percent for the small-scale poles. In the case of full-size poles, the average error rates were 4.3 and 3.1 percent for the high-order differential equation and Timoshenko models, respectively. All these show that the Timoshenko model was more accurate in predicting the deflection of both small- and full-size composite poles than the high-order differential equation

model. As shown in Equation 3.36, the constant in the Timoshenko model was approximated by a circular thick-shell cross-section in this study. In the actual application, the calculation of the Timoshenko constant was not an easy task, especially when the dimension of a cross-section changes with pole length, i.e., the cross-section of a tapered pole. There was no such a difficulty in the case of the high-order differential equation model. Since the dimension of the cross-section changes, k_8 and k_9 in Equation 3.16 are no longer constants and can be calculated by integration. This shows that the high-order differential equation is more suitable for analyzing complex pole geometries. The theoretical model for tapered composite poles is the next step of this study.

The deflection patterns for the full-size and small-scale composite poles under two levels of load conditions have been studied and plotted in Figures 3.4 to 3.7. As expected, the thinner shell thickness gave a greater deflection when both were subjected to the same load level. As stated in the previous shear analysis, the thinner shell also had greater shear and may not be neglected in the analysis. From the shear formula, it is known that the shear strength is dependent on the solid in the cross section area and moment of inertia. Filling the internal void in the poles may become necessary to compensate for the shear effects.

The effect of glue layers on deflection of a cantilever beam was analyzed for both reduced- and full-size composite poles and results show that glue-layer effects cannot be neglected. The strong effects are attributable to the high Young's modulus values of the adhesive. It is speculated that wood composite poles can be reinforced by introducing a thin layer of high strength material in the pole structure.

3.6 Summary and Conclusions

3.6.1 A Brief Summary of Model Development

In the analysis of solid and composite wood poles, cantilever bending test is the main testing method to obtain the poles' mechanical properties. Considering the cost of the poles and size of the testing equipment, it is necessary to develop models to assess these properties and thus facilitate research and applications. The hollow composite poles that are composed of multiple strips have never been studied. Thus, the main objective of this research was to develop a theoretical model using high-order differential equations to analyze and predict the deformation behavior and stress and strain characteristics of the composite poles with different strip thickness and NOS levels.

The present beam theories are derived from the classical and one-dimensional beam theory by formulating and solving high-order differential equations using the principle of minimum potential energy. In addition to the transverse shear effects, the uniform gravity load was included in the model. The Timoshenko beam theory was also derived to fit the conditions of composite pole analysis based on an energy method and to work as a comparison model with the high-order differential model. These models and analyses are the bases for further analysis of composite poles with a tapered form and joined strips.

The theoretical model was developed based on the Bernoulli-Euler theory and the Timoshenko beam theory. Assumptions made by these two theories were assumed in the derivation of the model. Glue layer effects were taken into account in the analysis. External forces were uniform body force and concentrated load on the free end. The total potential energy is the sum the potential energy of wood, glue layers, and the external

forces. The governing equations were derived and solved and the deformation function was obtained. The method provides solutions for the cantilever beam with a uniform load and/or concentrated load at the free end. The validation of the model was performed by substituting the Young's modulus and other loading conditions, and comparing the deflection results with those from the experiment.

3.6.2 Conclusions

Based on the analysis and results of this part of study, the following conclusions were made.

1. A high-order governing differential equation model was developed and verified by the experimental results. The correlation of the high-order governing differential equation model with the experimental results was very well.
2. The high-order governing differential equation model correlated well with the simplified beam model. The simplified model was more accurate than the high-order GDE model in predicting the deflection of composite poles.
3. The higher-order GDE model was more suitable for analyzing complex pole geometries.
4. Deflection of composite poles decreased with an increase of strip thickness or number of strips.
5. Glue layer deflection accounted for about 4 percent for the small-scale composite poles and about 5 percent for the full-size composite poles.
6. Laminated composite poles can be reinforced by introducing a thin layer of a high strength material in the pole structure.

7. Shear deflection accounted for 1 to 2 percent of total deflection for the small-scale composite poles, and 0.1 to 1 percent for the full-size composite poles.
8. Shear deformation can be effectively reduced by using filler materials in the hollow core of the fixed end.

3.7 References

Biblis, E.J. 1965. Shear deflection of wood beams. Forest Prod. J. 15(11):492-498.

Timoshenko, S. P. 1921. On the correction for shear of the differential equation for transverse vibrations of prismatic bars. Philosophical Magazine. 41(6):744-746.

Kant, T. and A. Gupta. 1988. A finite element model for a higher-order shear-deformable beam theory. Journal of Sound and Vibration. 125(2):193-202.

Rehfield, L. W. and P. L. N. Murthy. 1982. Toward a new engineering theory of bending: fundamentals. AIAA Journal. 20(5):693-699.

Kathnelson, A. N. 1996. Improved engineering theory for uniform beams. Acta Mechanica 114:225-229.

Shames, I. H. and C. L. Dym. 1985. Energy and finite element methods in structural mechanics. Hemisphere Publishing Corporation. 757 pp.

Washizu, K. 1968. Variational methods in elasticity and plasticity. Oxford, New York, Pergamon Press. 349pp.

Table 3.3. Comparison among the deflection values from experiment and theoretical models of small-scale composite poles with three strip-number levels and four thickness levels subjected to a 222 N (50 lbs) load.[1]

Strip Number	Strip thickness (cm)	Load (N)	Experiment deflection (cm)	HOD[2]		Timoshenko[3]	
				Predicted (cm)	Rate[4] (%)	Predicted (cm)	Rate[5] (%)
12	1.0	178	1.28	1.22	7.8	1.28	6.5
	1.5	178	1.07	1.00	6.7	1.05	2.3
	2.0	445	0.92	0.93	4.5	0.97	6.1
	2.5	445	0.93	0.86	7.5	0.90	3.6
9	1.0	178	1.92	1.74	6.7	1.82	3.4
	1.5	178	1.16	1.07	8.0	1.11	3.9
	2.0	445	1.38	1.31	4.6	1.37	2.0
	2.5	445	1.09	1.01	7.7	1.05	4.0
6	1.0	178	1.96	1.85	8.2	1.88	6.2
	1.5	178	1.94	1.91	6.3	1.98	11.0
	2.0	445	1.42	1.38	5.2	1.41	4.2
	2.5	445	1.25	1.23	3.9	1.27	4.0

[1] Tabled experiment and predicted deflection, and errors are the average of three values.
[2] High-order differential equation model.
[3] Timoshenko beam theory model.

Table 3.4. Comparison among the deflection values from experiment and theoretical models of the full-size composite poles with two strip-number levels and three thickness levels subjected to a 133 N (30 lbs) load.

Strip Number	Strip thickness (cm)	Experiment deflection (cm)	HOD[2]		Timoshenko[3]	
			Predicted (cm)	Rate (%)	Predicted (cm)	Rate (%)
12	1.9	8.94	9.28	3.7	9.05	1.1
	2.9	8.28	8.90	7.4	8.08	4.7
	3.8	6.71	7.07	5.9	6.87	2.9
9	1.9	10.90	10.48	3.8	10.25	6.0
	2.9	8.00	8.22	2.7	8.02	0.2
	3.8	9.77	9.62	2.1	9.39	3.8

[1] Tabled experiment and predicted deflection, and errors are the average of three values.
[2] High-order differential equation model.
[3] Timoshenko beam theory model.

Table 3.5. Comparison between the maximum bending stress values obtained in experiment and predicted by a high-order differential equation model of small-scale composite poles.

	Strip Thickness (cm)	1.0			1.5			2.0			2.5		
	Sample Number	1	2	3	1	2	3	1	2	3	1	2	3
6-Strip Poles	Theoretical (MPa)	58.71	59.84	58.35	63.61	59.14	74.99	86.16	75.35	70.88	92.05	93.40	93.76
	Experimental (MPa)	60.40	60.79	58.61	61.42	59.72	70.33	85.34	76.26	70.16	92.03	94.70	93.47
9-Strip Poles	Theoretical (MPa)	48.35	46.73	44.72	64.60	65.69	63.78	69.14	71.62	69.74	86.56	84.86	93.26
	Experimental (MPa)	48.24	46.13	44.91	65.49	67.26	66.49	70.22	67.72	68.57	87.95	84.50	95.37
12-Strip Poles	Theoretical (MPa)	44.10	33.30	44.30	55.45	44.05	52.09	84.91	75.82	72.93	92.91	69.57	89.78
	Experimental (MPa)	43.00	32.44	43.57	53.78	43.39	49.62	81.53	73.21	69.93	90.62	66.86	85.62

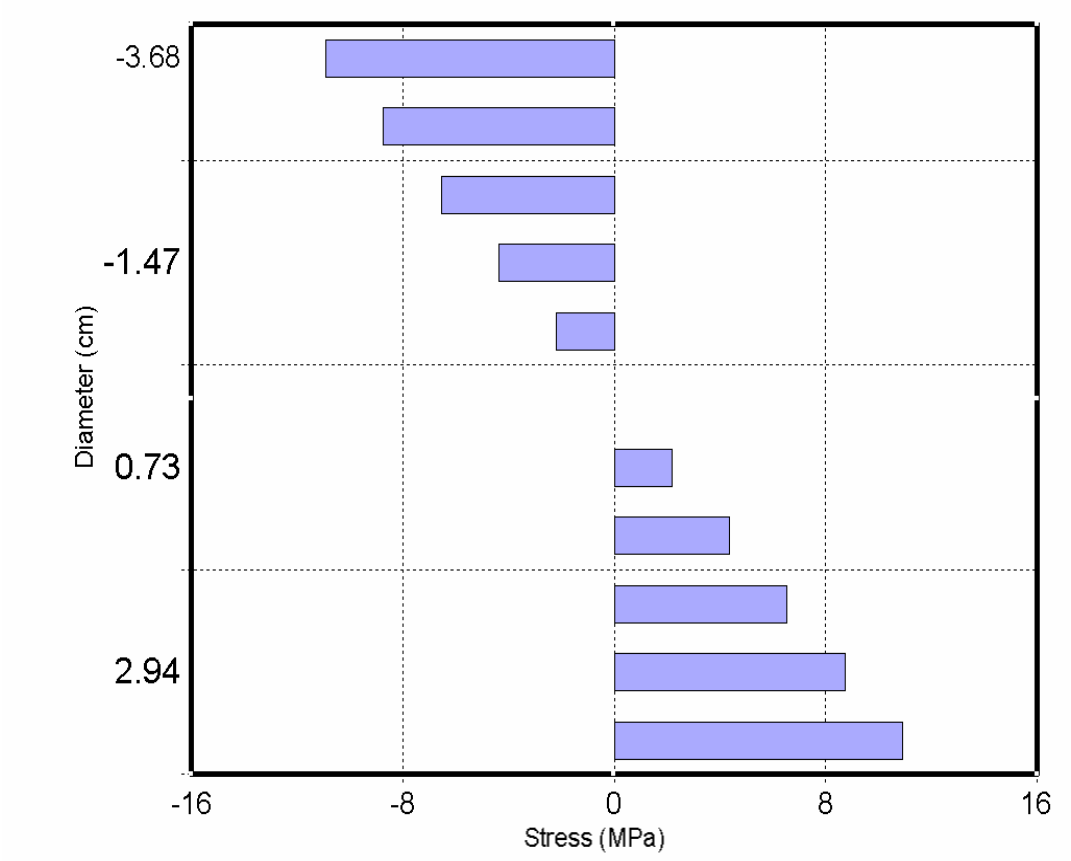

Figure 3.9. Stress distribution of small-scale composite poles with 12-sided and 2.0 cm (0.8 in) thickness subjected to a 445 N (100 lbs) concentrated load and a uniform body force.

CHAPTER 4

FINITE ELEMENT ANALYSIS

4.1 Introduction

Finite element analysis (FEA) is a computer-based finite element technique for solving a wide range of engineering problems. Problems in stress analysis, heat transfer, fluid flow, and electromagnetism may be solved or approximated by FEA. The basic concept is that a body or domain may be divided into smaller elements of finite dimensions called finite elements. The original body or domain is then considered as the assemblage of these elements and the continuous body or domain is visually discretized. The behavior of an individual element can be described with a relatively simple set of equations. The properties of the entire domain are then obtained through formulating and combining the equations of these elements. Thus, instead of solving the problem for the entire domain in one operation, the FEA procedure is mainly devoted to the formulation of properties of the constituent elements. This makes the FEA approach solve complex engineering problems, mathematical solution of which is tedious and usually not possible by analytical methods. In the mechanical analysis of a beam, FEA can be used to calculate deflection, stress, vibration, buckling behavior and many other phenomena. Either small or large-scale deflection under loading or applied displacement can be analyzed by FEA. A computer is required in FEA because of the astronomical number of calculations needed to analyze a large structure.

FEA is done principally by commercially purchased software. ANSYS is one of the large-scale, general-purpose finite element computer programs. First released in

1971, ANSYS has been a leading FEA program for over 20 years (Moaveni 1999). It can be used for the solution of several classes of engineering analyses. Some of them are static and dynamic analyses; elastic, plastic, creep and swelling; small and large deflections; steady state and transient heat transfer. ANSYS Graphical User Interface (GUI), pull-down menu, dialog boxes, and a tool bar make analysis simple to perform. It is a useful tool in FEA.

The objective of this part of study is to do FEA of wood laminated composite poles with ANSYS. Deflection, stress and strain for different configurations of poles subjected to concentrated and body forces were obtained using ANSYS. The FEA results were compared with those from the experiment and the theoretical study.

4.2 Basic Theories

Considering a body as composed of finite elements which are connected at specified node points is the basic idea of the finite element method. Since the variation of displacement inside the body is not known, it is assumed that the displacement variation in a finite element can be approximated by a simple function or interpolation function in terms of the nodal values of the element. The solution of the system equations gives the unknown nodal values and the solution within any finite element in the body will be known. In this analysis, the interpolation functions are linear polynomials and have the following form

$$\phi(x, y, z) = \alpha_1 + \alpha_2 x + \alpha_3 y + \alpha_4 z \tag{4.1}$$

The element type was hexahedron assembled by five tetrahedrons, which have four nodes. Let the i, j, k, and l represent the four nodes and (x_i, y_i, z_i), (x_j, y_j, z_j), (x_k, y_k, z_k),

and (x_l, y_l, z_l) the coordinates at nodes i, j, k, l. Then the displacement model within an element "e" can be expressed as

$$\vec{T} = \begin{Bmatrix} u(x,y,z) \\ v(x,y,z) \\ w(x,y,z) \end{Bmatrix} = \left[N(x,y,z) \right] \vec{\phi}^{(e)} \tag{4.2}$$

where $N(x, y, z)$ is called shape function and has the following expression

$$N(x,y,z) = \begin{bmatrix} N_i & 0 & 0 & N_j & 0 & 0 & N_k & 0 & 0 & N_l & 0 & 0 \\ 0 & N_i & 0 & 0 & N_j & 0 & 0 & N_k & 0 & 0 & N_l & 0 \\ 0 & 0 & N_i & 0 & 0 & N_j & 0 & 0 & N_k & 0 & 0 & N_l \end{bmatrix}$$

$$N_i = \frac{1}{6V}(a_i + b_i x + c_i y + d_i z)$$

$$N_j = \frac{1}{6V}(a_j + b_j x + c_j y + d_j z)$$

$$N_k = \frac{1}{6V}(a_k + b_k x + c_k y + d_k z)$$

$$N_l = \frac{1}{6V}(a_l + b_l x + c_l y + d_l z)$$

and

$$\vec{\phi}^{(e)} = \left\{ u_i v_i w_i u_j v_j w_j u_{ik} v_k w_k u_l v_l w_l \right\}^T$$

$$V = \frac{1}{6} \begin{vmatrix} 1 & x_i & y_i & z_i \\ 1 & x_j & y_j & z_j \\ 1 & x_k & y_k & z_k \\ 1 & x_l & y_l & z_l \end{vmatrix} \qquad a_i = \begin{vmatrix} x_j & y_j & z_j \\ x_k & y_k & z_k \\ x_l & y_l & z_l \end{vmatrix}$$

$$b_i = \begin{vmatrix} 1 & y_j & z_j \\ 1 & y_k & z_k \\ 1 & y_i & z_i \end{vmatrix} \qquad c_i = \begin{vmatrix} x_j & 1 & z_j \\ x_k & 1 & z_k \\ x_l & 1 & z_l \end{vmatrix}$$

$$d_i = \begin{vmatrix} x_j & y_j & 1 \\ x_k & y_k & 1 \\ x_l & y_l & 1 \end{vmatrix} \qquad \text{et al.}$$

In the formulation of differential equations, the principle of minimum potential energy was used. The strain energy may be expressed as follows

$$U_\sigma = \frac{1}{2}\iiint_V \bar{\epsilon}^T \, \sigma dV \tag{4.3}$$

$$\vec{\sigma} = \left[\sigma_{xx}\sigma_{yy}\sigma_{zz}\sigma_{xy}\sigma_{yz}\sigma_{xz}\right]^T = [D]\,\bar{\epsilon} \tag{4.4}$$

where

$$\bar{\epsilon} = \left[\epsilon_{xx}\epsilon_{yy}\epsilon_{zz}\epsilon_{xy}\epsilon_{yz}\epsilon_{xz}\right]^T$$

$$[D] = \begin{bmatrix} \frac{E_L}{K}(1-\upsilon_{RT}\upsilon_{TR}) & \frac{E_L}{K}(\upsilon_{RL}+\upsilon_{RT}\upsilon_{TL}) & \frac{E_L}{K}(\upsilon_{TL}+\upsilon_{RL}\upsilon_{TR}) & 0 & 0 & 0 \\ \frac{E_R}{K}(\upsilon_{RL}+\upsilon_{LT}\upsilon_{TR}) & \frac{E_R}{K}(1-\upsilon_{LT}\upsilon_{TL}) & \frac{E_R}{K}(\upsilon_{TR}+\upsilon_{LR}\upsilon_{TL}) & 0 & 0 & 0 \\ \frac{E_T}{K}(\upsilon_{LT}+\upsilon_{LR}\upsilon_{RT}) & \frac{E_T}{K}(\upsilon_{RT}+\upsilon_{RL}\upsilon_{LT}) & \frac{E_T}{K}(1-\upsilon_{LR}\upsilon_{RL}) & 0 & 0 & 0 \\ 0 & 0 & 0 & G_{LR} & 0 & 0 \\ 0 & 0 & 0 & 0 & G_{LT} & 0 \\ 0 & 0 & 0 & 0 & 0 & G_{RT} \end{bmatrix}$$

$$K = 1 - \upsilon_{RT}\upsilon_{TR} - \upsilon_{RL}\upsilon_{LR} - \upsilon_{LT}\upsilon_{TT} - \upsilon_{RL}\upsilon_{LT}\upsilon_{TR} - \upsilon_{RT}\upsilon_{TL}\upsilon_{LR}$$

E_L, E_R, and E_T are the modulus of elasticity of the wood and υ_{LR}, υ_{TR}, υ_{LT}, et al. are the Piosson's ratios. The strain vector $\bar{\epsilon}$ can be expressed in terms of the nodal displacement vector $\vec{\phi}^{(e)}$ by differentiating Equation 4.2 as

$$\vec{\epsilon} = \begin{bmatrix} \epsilon_{xx} \\ \epsilon_{yy} \\ \epsilon_{zz} \\ \epsilon_{xy} \\ \epsilon_{yz} \\ \epsilon_{xz} \end{bmatrix} = \begin{bmatrix} \partial u/\partial x \\ \partial v/\partial y \\ \partial w/\partial z \\ \partial u/\partial y + \partial v/\partial x \\ \partial v/\partial z + \partial w/\partial y \\ \partial w/\partial x + \partial u/\partial z \end{bmatrix} = \begin{bmatrix} \frac{\partial}{\partial x} & 0 & 0 \\ 0 & \frac{\partial}{\partial y} & 0 \\ 0 & 0 & \frac{\partial}{\partial z} \\ \frac{\partial}{\partial y} & \frac{\partial}{\partial x} & \\ & \frac{\partial}{\partial z} & \frac{\partial}{\partial y} \\ \frac{\partial}{\partial z} & & \frac{\partial}{\partial x} \end{bmatrix} \begin{bmatrix} u \\ v \\ w \end{bmatrix} = [B]\vec{\phi}^{(e)} \tag{4.5}$$

where

$$[\boldsymbol{B}] = \begin{bmatrix} \frac{\partial}{\partial x} & \mathbf{0} & \mathbf{0} \\ \mathbf{0} & \frac{\partial}{\partial y} & \mathbf{0} \\ \mathbf{0} & \mathbf{0} & \frac{\partial}{\partial z} \\ \frac{\partial}{\partial y} & \frac{\partial}{\partial x} & \\ & \frac{\partial}{\partial z} & \frac{\partial}{\partial y} \\ \frac{\partial}{\partial z} & & \frac{\partial}{\partial x} \end{bmatrix} [\boldsymbol{N}]$$

The work done by the body force may be expressed as followings

$$\boldsymbol{U_b} = -\iiint_V \vec{\boldsymbol{T}}^{\boldsymbol{T}} \vec{\boldsymbol{P}}_{\boldsymbol{b}} \boldsymbol{dV} = -\iiint_V \vec{\boldsymbol{\phi}}^{(e)^{\boldsymbol{T}}} [\boldsymbol{N}]^{\boldsymbol{T}} \vec{\boldsymbol{P}}_{\boldsymbol{b}} \boldsymbol{dV} \tag{4.6}$$

where $\vec{P}_b$ is the vector of body forces per unit volume. The work done by a concentrate load is as

$$\boldsymbol{U_c} = -\vec{\boldsymbol{\phi}}^{(e)^{\boldsymbol{T}}} \vec{\boldsymbol{P}}_{\boldsymbol{c}} \tag{4.7}$$

Then the strain energy of the whole pole may be as

$$U_s = \sum_{e=1}^{n} U\sigma = \frac{1}{2}\sum_{e=1}^{n}\left[\iiint_V \vec{\varphi}^{(e)T}[B]^T[D][B]\vec{\varphi}^{(e)}dV\right] \tag{4.8}$$

and the work of body force for the whole pole is as

$$U_B = \sum_{e=1}^{n} U_b = \sum_{e=1}^{n}\left[-\iiint_V \vec{\phi}^{(e)T}[N]\vec{P}_b dV\right] \tag{4.9}$$

Thus, the total potential energy for the pole is

$$\pi = \frac{1}{2}\sum_{e=1}^{n}\left[\iiint_V \vec{\phi}^{(e)T}[B]^T[D][B]\vec{\phi}^{(e)}dV\right] - \iiint_V \vec{\phi}^{(e)T}[N]^T\vec{P}_b dV - \vec{\phi}^{(e)T}\vec{P}_c \tag{4.10}$$

It is noted that $\vec{\phi}^{(e)}$ in Equation 4.10 can be replaced by $\vec{\phi}$ if remaining element matrices are enlarged by adding their required number of zero elements, thus

$$\pi = \frac{1}{2}\sum_{e=1}^{n}\left[\iiint_V \vec{\phi}^{T}[B]^T[D][B]\vec{\phi}dV\right] - \iiint_V \vec{\phi}^{T}[N]^T\vec{P}_b dV - \vec{\phi}^{T}\vec{P}_c \tag{4.11}$$

According to the principle of minimum potential energy, the system is in equilibrium if the first derivative of total potential energy equal zero. The following equation must be met:

$$\frac{\partial\pi}{\partial\phi_1} = \frac{\partial\pi}{\partial\phi_2} = \frac{\partial\pi}{\partial\phi_3} = \ldots = \frac{\partial\pi}{\partial\phi_M} = 0 \tag{4.12}$$

where *M* is the total number of nodal displacements or degree of freedom. From Equations 4.11 and 4.12, we obtained

$$\left(\sum_{e=1}^{n}\left[\iiint_V [B]^T[D][B]dV\right]\right)\vec{\phi} = \iiint_V [N]^T\vec{P}_b dV - \vec{P}_c \tag{4.13}$$

Let

$$K^{(e)} = \iiint_V \vec{\phi}^T [B]^T [D][B]\vec{\phi}\, dV$$

$$\vec{P}_B = \iiint_V \vec{\phi}^T [N]^T \vec{P}_b dV$$

Equation 4.13 becomes

$$\left(\sum_{e=1}^{n} K^{(e)} \right) \vec{\phi} = \sum_{e=1}^{n} \vec{P}_B + \vec{P}_c \tag{4.14}$$

$\left(\sum_{e=1}^{n} K^{(e)} \right)$ is the assembled stiffness matrix, and $\sum_{e=1}^{n} \vec{P}_B + \vec{P}_c$ is the assembled nodal load vector. The required solution for the nodal displacements and element stresses can be obtained after solving Equation 4.14.

4.3. Discretization of the Domain

The discretization of the pole shell domain is automatically conducted by ANSYS once the necessary parameters are set. After the element edge length is filled in the dialog box, the ANSYS discretizes each strip in the pole by the 'Mesh' command. In this analysis, the element edge length was set as 1.27 cm (0.5 in) for small-scale poles and 2.54 cm (1 in) for full-size composite poles. According to this specification, ANSYS meshed small-scale shells of the 2.54-cm-thick-strip poles into three layers, and two layers for the 2.0-cm-thick-strip poles, and one for other two thickness levels. The strip width of the 12-strip poles was about 2.0 cm (0.8 in) and the ANSYS meshed it two parts, and the width of each 9- and 6-strip was meshed into three elements. Each element in the domain was a hexahedron with element edges less than 2.54 cm (1 in). The number of elements for each configuration and length level is presented in Table 4.1. Figure 4.1 shows the discretization of a 9-strip pole with 2.54 cm strip thickness.

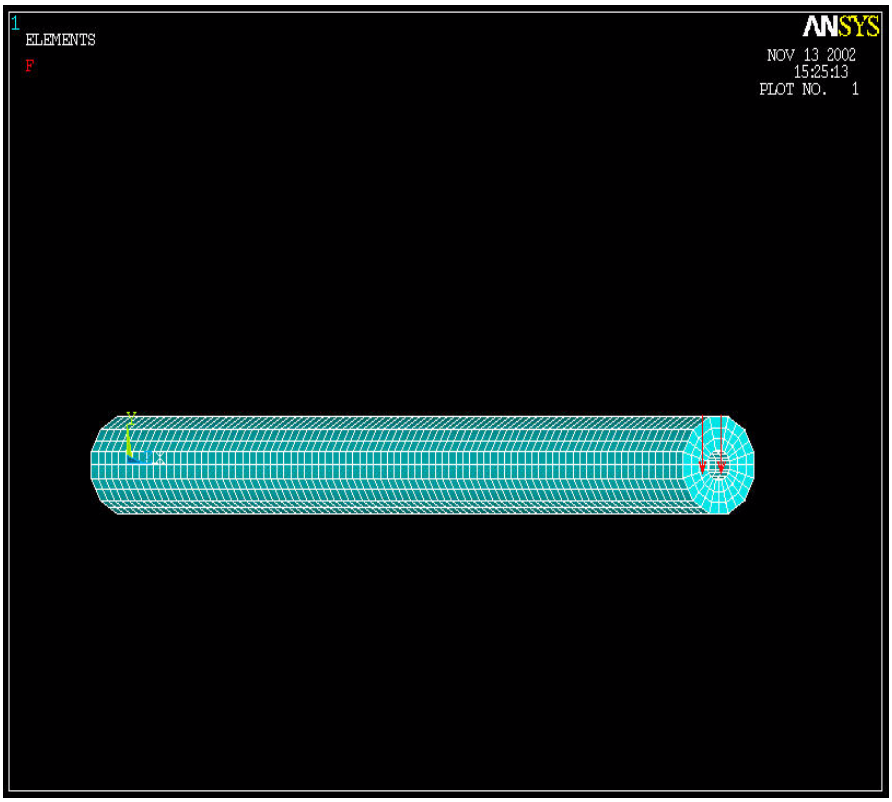

Figure 4.1. Discretization and application of loads in the finite element analysis of wood composite poles using ANSYS.

Table 4.1. The number of elements in each configuration of composite poles.

Strip	107-cm pole			549-cm pole	
thickness	6	9	12	9	12
2.54	1008	1512	1008	10404	15862
2.03	504	756	504	9888	14214
1.52	504	756	504	7004	8832
1.01	504	756	504	-	-

4.4 Material Properties

The material properties of southern yellow pine (SYP) were determined through testing clear wood samples according to ASTM D 143-94. The wood was taken from the same batch of materials used in the manufacture of composite poles and solid poles. The sample size was 25 x 25 x 410 mm (1 x 1 x 16 in). Loading span was 35 cm (14 in) and

loading speed was 1.25 mm/min (0.05 in/min). A total of 35 specimens were tested. The average values of modulus of rupture (MOR) were 102 MPa (14.8 kpsi) with standard deviation of 13.5 MPa, and the average of modulus of elasticity (MOE) was 10,872 MPa (1.58 Mpsi) with standard deviation of 2,017 MPa. Other properties of SYP were taken from references and listed in Table 4.2.

Table 4.2. Selected mechanical properties of clear southern yellow pine wood.[1]

Strength properties (10^6 psi)					Poisson's Ratios		
E_R	E_T	G_{LR}	G_{LT}	G_{RT}	ν_{LR}	ν_{LT}	ν_{RT}
0.1487	0.0971	0.1200	0.1109	0.01318	0.37	0.42	0.47

[1] Bodig and Jayne (1982).

4.5 ANSYS Procedures

There are two phases in the analysis using ANSYS, i.e., processing and solution phases. In the processing phase, the problem to be analyzed is defined. The steps in this phase include:

1. Create keypoints. The keypoints in ANSYS are to delineate the overall geometry by specifying various principle coordinates to define the body. The point coordinates of the 6-, 9-, and 12-sided polygons were calculated and input into the computer. Since the poles are hollow, a smaller polygon situates in the inside of the bigger one, thus the keypoints of the smaller one are also calculated and drawn. The units used throughout the analysis were centimeter of the metric system.

2. Form lines. After the keypoints are defined, lines are drawn between the keypoints to form the geometry of the polygons. The corresponding keypoints between the outside and inside polygons are also connected by lines to form the trapezoid of the cross section of the strip.
3. Form areas. The trapezoid areas are formed by four lines to represent the cross section of strips and poles.
4. Define the type of element. ANSYS predefines various element type to cope with the actual application environments. The type of element selected in this study was Solid 64 in ANSYS. It is a three-dimensional solid with anisotropic properties.
5. Element material properties. There are nine material properties to be defined in Element Solid 64. They are modulus of elasticity, modulus of rigidity, and Poisson's ratios in x, y, and z directions. Table 4.2 lists some of these properties that were used in this study. Since the body force was taken into account in the analysis, the density of the poles was defined.
6. Extrude the area. ANSYS has the tools to form a solid from areas by extruding or sweeping the base area. In this study, the cross section of the poles was extruded to the designed length for both the full-size and small-scale composite poles and solid pole shells were formed.
7. Mesh size. This step is to tell ANSYS how big the elements should be. In this analysis, the element size for small-scale configurations was 1.27 cm (0.5 in) and the element size for full-size poles was 2.54 cm (1.0 in). These sizes were about the width of the larger side of the strips in both kinds of poles.

8. Mesh. This step is to mesh the body according to the element size chosen. This is an automatic process in which the specified domain is divided into small elements. ANSYS will number each node and element in the meshed solid.

The next phase is the solution phase. There are four steps in this phase. They are:

1. Define the analysis type. There are 7 types of analysis to be chosen in ANSYS. In the case of this study, static was selected as the analysis type.
2. Apply constraints. It is necessary to apply constraints to the model so that singular solution may result. Some of these constraints are the boundary conditions of the problem. For this study, the degree of freedom of the fixed end was set to zero.
3. Apply loads. This step allows loads to be applied to the body defined in three dimensions. In this study, two kinds of loads were applied. They were the concentrated load on the free end and gravity. To balance the load applied on the pole, the specific load values were divided by two, each of which was applied on one of the two nodes on the top strip of each pole and both nodes were situated in the same cross section.
4. Solving the system. This is the last step of the analysis. If all the parameters required are specified and all procedures are correct, ANSYS will solve the problem and give the results.

ANSYS presents the analysis results in lists or figures. Some of the list results include deformation, stress, and strain on each of the nodes defined. The plot results include deformation, stress and strain distribution, moment, and element and node information.

4.6 Experimental Study

The preparation of materials, samples, and tests of full-size and small-scale composite poles are referred to Chapters 2 and 3. Both small-scale and full-size composite poles were analyzed by the finite element method. To compare the strain in experimental study and the strain predicted by the finite element method, strain gages were attached to the full-size composite poles. Strain gages were not installed on the small-scale composite poles.

For the consideration of comparison, in the finite element analysis the Young's modulus in the longitudinal direction (z direction) of each full- or small-scale pole was the experimental values in Chapter 2. Other material properties are listed in Table 4.2.

4.7 Results

4.7.1 Results of Finite Element Solutions

Some of the ANSYS results are shown in Figures 4.2 to 4.4. Figure 4.1 shows that a composite pole was discretized into tetrahedron elements. Loads and constraints were added and the system was ready to be solved for solutions. The node and element numbering systems of ANSYS are shown in Figure 4.2. Figures 4.3 and 4.4 give the plots of results of deformation and stress distribution.

The variations of deflection for reduced- and full-size composite poles are plotted in Figures 4.5 and 4.6. All small-scale composite poles were subjected to 222 N (50 lbs) of load on the free end. Figure 4.6 shows the trend of deflection of full-size composite poles, which were loaded to 133 N (30 lbs). In both cases, the thinner shell poles deflected more.

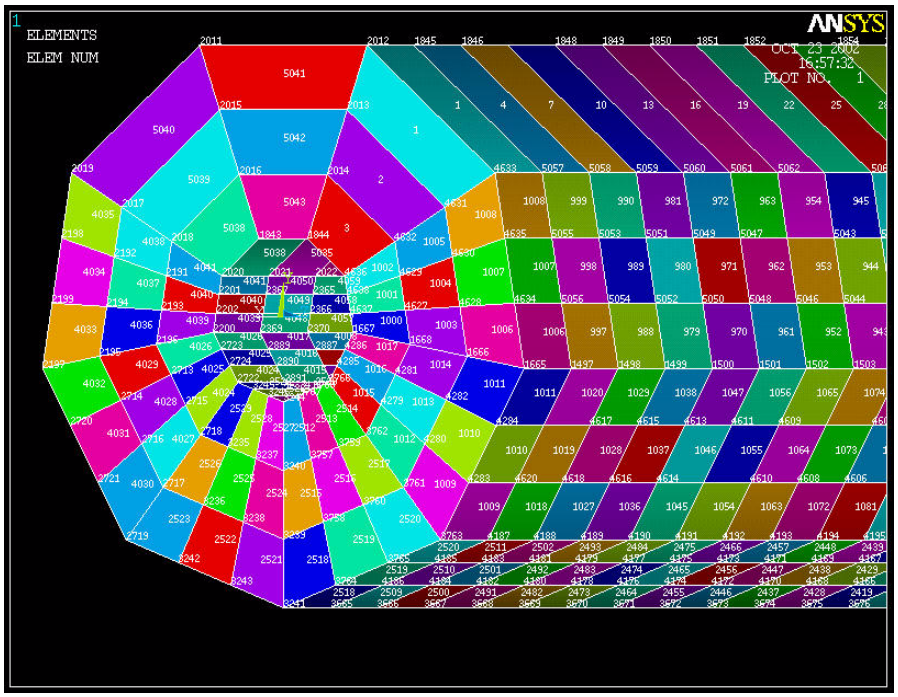

Figure 4.2. An ANSYS numbering system in the finite element analysis of wood composite poles.

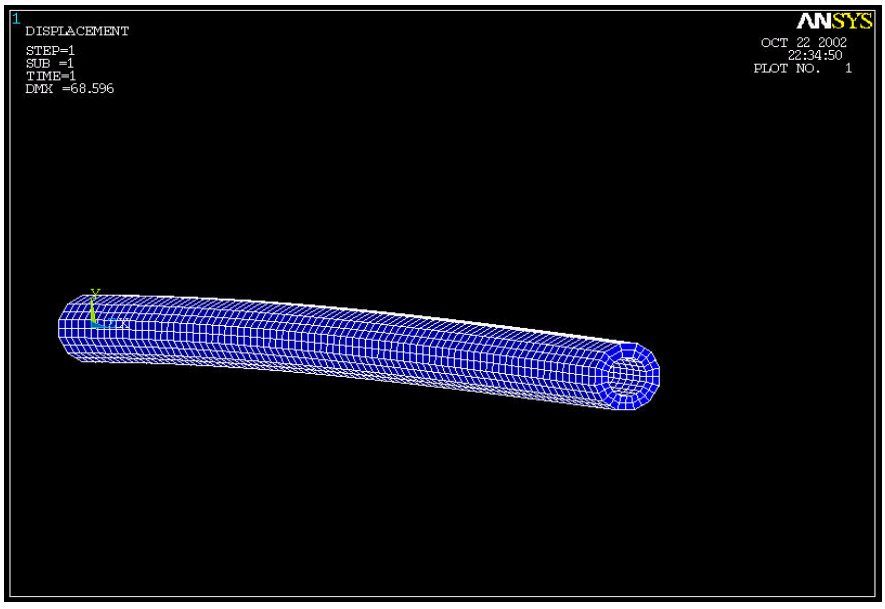

Figure 4.3. Deformation of a wood composite pole in the solution of finite element analysis using ANSYS.

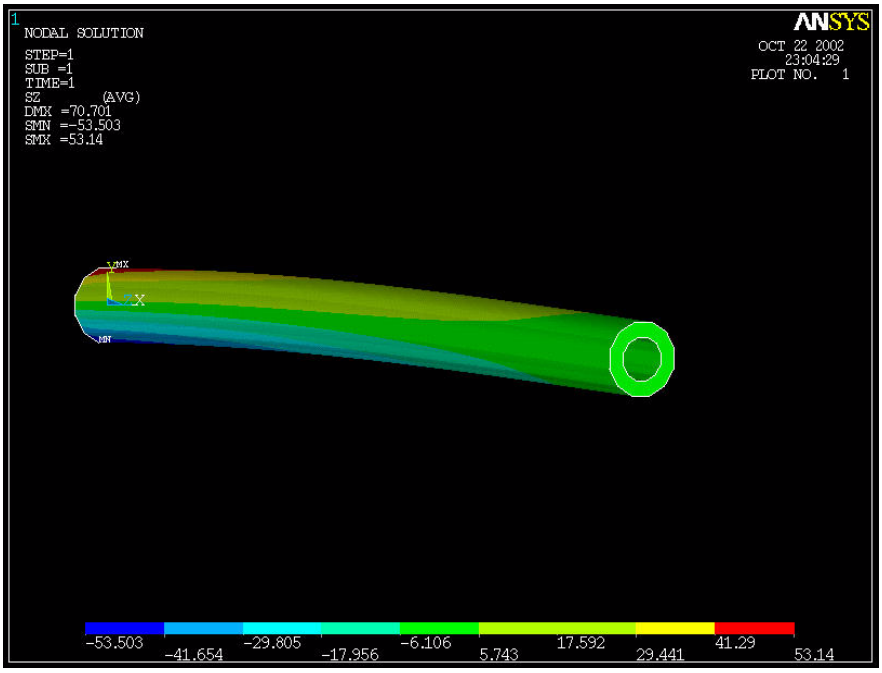

Figure 4.4. Stress distribution of a wood composite pole in the finite element analysis using ANSYS.

The variations of stress and strain of the small-scale composite poles are displayed in Figures 4.7 and 4.8. Figure 4.7 shows increases of stress as nodal numbers moving toward the support. It also shows that the maximum bending stress increased rapidly with an increase of strip thickness. In the case of strain, since greater stress causes bigger strain, the thin strips gave more strain, as shown in Figure 4.8.

4.7.2 Comparison with Experimental Results

Results obtained from the finite element analysis were compared with those from the experimental study. For the comparison between deflections, the experimental data was obtained from the load-deflection graphs in the experimental test in Chapter 2. The description of the test was described in Chapter 2. The load level of each small-scale

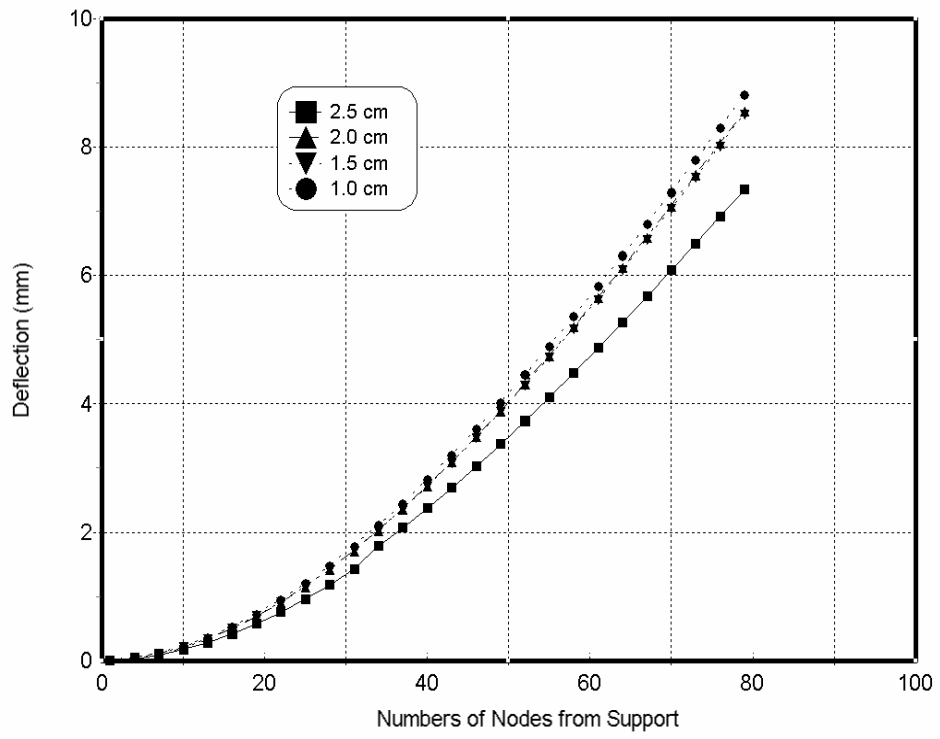

Figure 4.5. Deflection of 12-sided small-scale composite poles predicted by a finite element model.

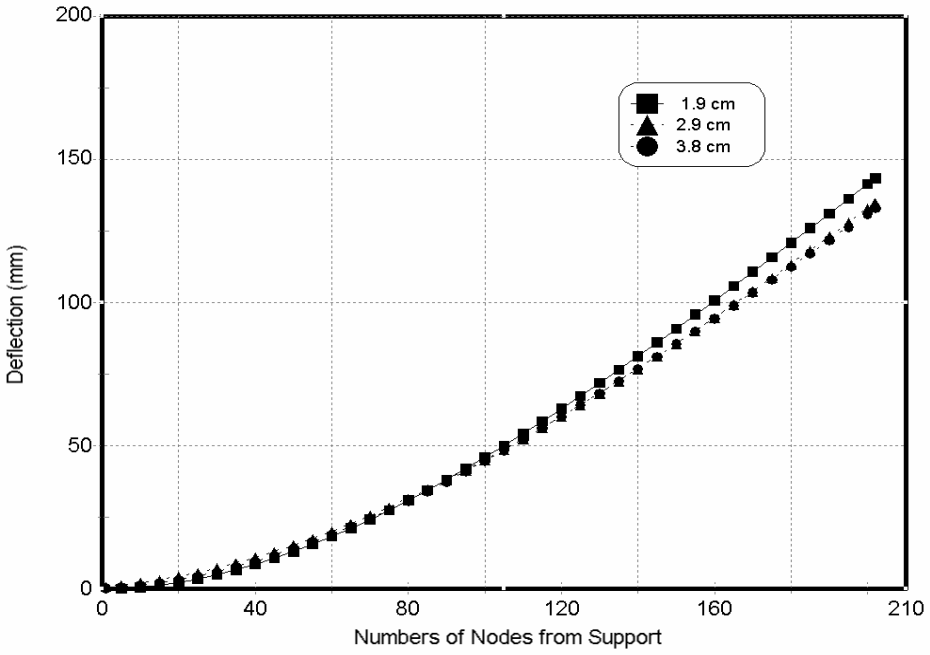

Figure 4.6. Deflection of 12-strip full-size composite poles predicted by a finite element model.

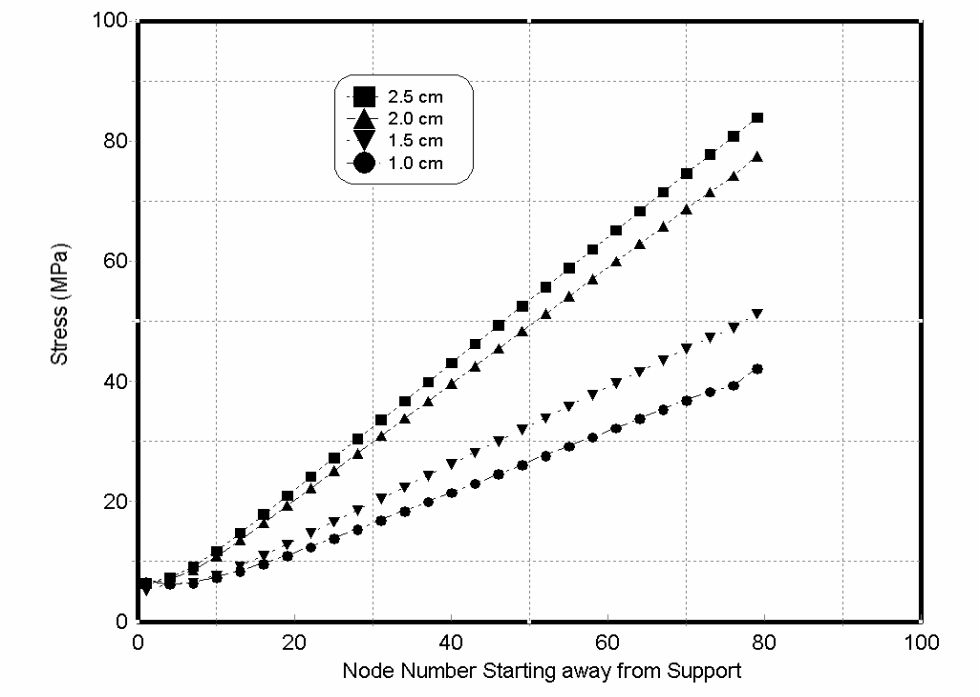

Figure 4.7. Maximum bending stress of small-scale 12-sided composite poles with 4 strip thickness levels. Predicted by a finite element model.

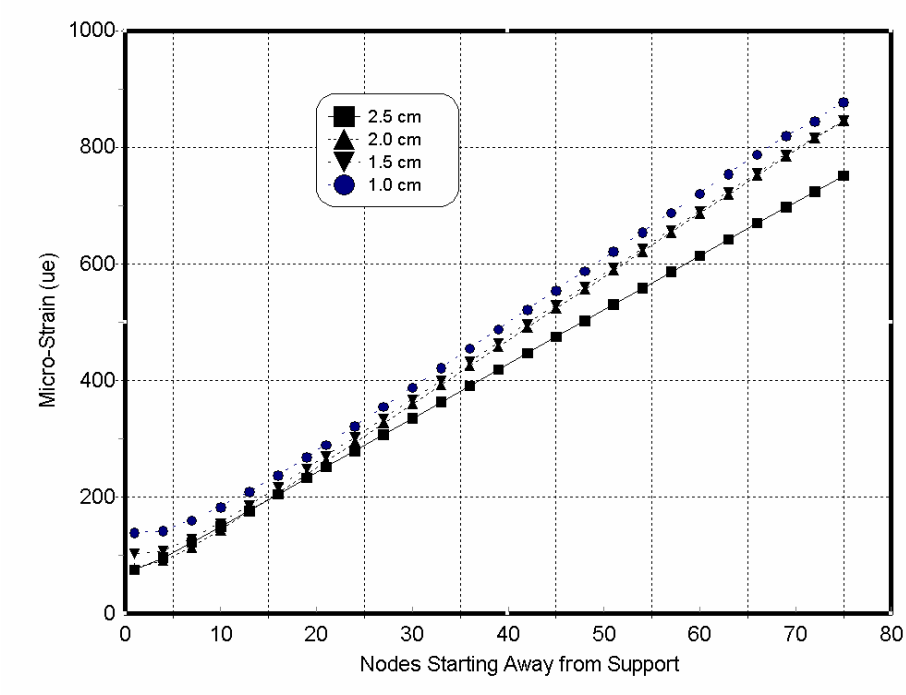

Figure 4.8. Strain of 12-strip small-scale composite poles predicted by a finite element model under a 133 N (30 lbs) concentrated load.

composite pole was the same and equaled 222 N (50 lbs) for both FEM and experiment study. For the full-size poles, the load was 133 N (30 lbs). Tables 4.3 and 4.4 give the results obtained from the two tests. Most experimental values were higher than the finite element analysis values for the small-scale composite poles. Except for some samples in the 1.0 and 1.5 cm thickness levels, experimental values agreed well with those of finite element analyses. The deflection of full-size composite poles obtained from the finite element analysis also correlated well with the experiment.

Table 4.5 presents the comparison between maximum bending stress values obtained from experiment and from the finite element analysis. Finite element analysis values mostly were 2 to 6 percent higher than the experimental ones. The higher errors occurred in the thinner shell range and in the 12-strip poles. The maximum bending stress decreased as the strips became thinner.

The strain values of full-size composite poles along with their finite-elementally predicted values are shown in Table 4.6. The correlation was poor and the finite element results were higher than values from experiment.

4.7.3 Comparison with Theoretical Results

Comparisons were also made between the theoretical and finite element models. Table 4.7 lists the deflection values predicted by both models for the small-scale composite poles. Variations existed between the values predicted by the two models and the biggest variation is found in the 1.0 strip thickness level. The difference between the two models was about 1 percent of their original values. Table 4.8 lists the deflection

Table 4.3. Comparison between the deflection values obtained in the experiment and values predicted from finite element analyses of small-scale composite poles subjected to a 222 N (50 lbs) load.

	Strip Thickness (cm)	**1.0**			**1.5**			**2.0**			**2.5**		
	Samples	1	2	3	1	2	3	1	2	3	1	2	3
6-Strip	Experiment (mm)	18.88	20.04	19.29	13.61	20.80	23.63	15.13	13.33	14.18	12.29	12.19	13.14
Poles	FEM Analysis (mm)	16.03	17.86	19.59	11.36	24.08	24.53	14.83	12.54	14.91	13.03	15.88	13.36
9-Strip	Experiment (mm)	19.47	18.91	18.55	12.48	11.63	10.59	10.40	17.02	13.90	10.59	11.82	10.40
Poles	FEM Analysis (mm)	18.24	19.72	17.36	12.41	11.41	9.74	10.52	17.54	13.51	10.17	11.93	9.63
12-Strip	Experiment (mm)	13.61	13.61	10.97	10.40	9.83	11.91	8.70	8.98	10.00	8.51	9.61	9.83
Poles	FEM Analysis (mm)	9.97	9.25	11.73	8.39	6.84	9.37	9.80	9.41	9.89	8.21	9.16	9.68

Table 4.4. Comparison between the deflection values obtained experimentally and the values predicted by the finite element method of the full-size composite poles subjected to the same load for both test methods.

	Strip Thickness (cm)	**1.91**	**1.91**	**2.86**	**2.86**	**3.81**	**3.81**
	Load (N)	133	133	133	133	133	133
9-Strip Poles	Experiment (cm)	13.02	8.89	9.14	7.95	9.19	9.34
	FEM Test (cm)	12.31	8.83	8.27	7.94	9.84	9.23
12-Strip Poles	Experiment (cm)	10.03	8.64	7.80	8.15	7.72	6.87
	FEM Test (cm)	9.13	8.80	8.43	8.56	7.89	6.83

Table 4.5. Comparison between the maximum bending stress values obtained in experiment and predicted by a finite element method of small-scale composite poles.

	Strip Thickness (cm)	**1.0**			**1.5**			**2.0**			**2.5**		
	Samples	1	2	3	1	2	3	1	2	3	1	2	3
6-Strip	Experiment (MPa)	60.40	60.79	58.61	61.42	59.72	70.33	85.34	76.26	70.16	92.03	94.70	93.47
Poles	FEM Analysis (MPa)	63.19	63.21	60.65	63.99	60.29	70.92	86.08	76.48	70.81	92.91	94.99	93.35
9-Strip	Experiment (MPa)	48.24	46.13	44.91	65.49	67.26	66.49	70.22	67.72	68.57	87.95	84.50	95.37
Poles	FEM Analysis (MPa)	49.51	47.16	46.33	67.21	69.29	69.04	71.31	67.57	69.01	88.07	84.19	95.72
12-Strip	Experiment (MPa)	43.00	32.44	43.57	53.78	43.39	49.62	81.53	73.21	69.93	90.62	66.86	85.62
Poles	FEM Analysis (MPa)	47.21	35.81	47.28	57.88	47.25	53.14	85.98	77.36	73.77	95.58	70.35	89.8

obtained from the analysis of full-size composite poles. As shown in the Table, the difference between the two models was in the same order as the small-scale poles.

Table 4.9 gives the comparison between the maximum bending stress values obtained from the two models for the small-scale poles. The stress values predicted by the finite element model were 1 to 6 percent higher than the theoretical ones.

4.8 Discussion

Distribution of the deflection values from experiment, theoretical analysis and FEM of the small-scale composite poles with 12 strips is plotted in Figure 4.9. The data values from two models were close to the experimental values. In both the theoretical and finite element analyses, transverse shear was included in the models and the errors in the models were reduced. Since the experimental Young's modulus was used in the formation of both models, both models predicted the same specific data points, which were the experimental values. Thus the fluctuation of data points in Figure 4.9 was due to the difference of Young's modulus among the samples in one group and between groups as well as the thickness effect. The experimental values were higher than both the theoretical and finite element values. The poor correlations between the experimental values and those of the FEM model in the 1.0 cm and 1.5 cm thickness ranges were due to the plastic deformation of the poles. Table 4.10 gives the comparisons in two thickness levels when the load was set to 89 N (20 lbs). The accuracy was improved when a lower load was added.

As shown in Figure 4.4, the maximum bending stress occurred in the parabolic areas on top and bottom skins near the fixed end, where all degrees of freedoms are zero. On the top skin, the stress is in tension, whereas on the bottom compression. This results

in elevated shear in the central plane. The low maximum bending stress of thin shell poles, as shown in Figure 4.7 and Table 4.5, is partially due to the shear breakage in either the clamped area or in the cantilever part. Shear breakage might be one of the main failure styles for thin shell poles.

The correlation of finite element values to those of experiment was around 2 to10 percent, and to those of theoretical results was 1 to 5 percent.

4.9 Conclusions

Finite element analysis was conducted on reduced- and full-size composite poles using ANSYS. The finite element results were compared to experimental values and theoretical results. Based on these results, the following conclusions were made:

1. The accuracy of the finite element results was first verified by the experiment data. The correlations are found to be good. The experimental values in deflection were 2 to 10 percent higher than the finite element ones. The maximum bending stress values show the same trend.
2. The accuracy of the finite element results was then correlated to the results obtained from the theoretical study. The theoretical values were 1 to 5 percent higher than the finite elemental ones. Maximum bending stress values predicted by the finite element model were greater than those obtained from the theoretical study.
3. Maximum bending stress of composite poles in the cantilever test was in the parabolic areas on the top and bottom skins near the fixed end. The shear on the central plane between the two maximum bending stress areas reaches maximum and shear failure may be the main breakage style for the thin shell poles.

4.10 References

American Society for Testing and Materials. 1998. Standard methods of testing small clear specimens of timber, D 143-94.

Bodig, J., A.J. Benhamin. 1982. Mechanics of wood and wood composites. Van Nostrand Reinhold, New York. 712p.

Moaveni, S. 1999. Finite element analysis: Theory and application with ANSYS. Prentice Hall, Upper Saddle River, N.J. 527p.

Table 4.6. Comparison of strain values obtained from attached strain gages with those predicted from finite element analyses of the full-size composite poles.

	Strip Thickness (cm)	**1.91**	**1.91**	**2.86**	**2.86**	**3.81**	**3.81**
9-Strip Poles	Experiment (ue*)	496	513	416	556	494	397
	Finite Element Analysis (ue)	622	646	504	731	615	503
12-Strip Poles	Experiment (ue)	614	513	459	460	464	429
	Finite Element Analysis (ue)	701	647	533	505	515	522

* micro-strain (10^{-6}).

Table 4.7. Comparison between the deflection values obtained in the theoretical analysis and values predicted from finite element analyses of small-scale composite poles subjected to a 222 N (50 lbs) load.

	Strip Thickness (cm)	**1.0**			**1.5**			**2.0**			**2.5**		
	Samples	1	2	3	1	2	3	1	2	3	1	2	3
6-Strip	Theoretical (mm)	16.08	18.54	21.00	11.02	23.07	23.23	14.38	12.18	14.45	12.67	11.34	12.94
Poles	FEM Analysis (mm)	16.03	17.86	19.59	11.36	24.08	24.53	14.83	12.54	14.91	13.03	15.88	18.36
9-Strip	Theoretical (mm)	17.21	18.57	16.40	11.81	10.88	9.30	10.40	16.49	12.85	9.74	11.37	9.24
Poles	FEM Analysis (mm)	18.24	19.72	17.36	12.41	11.41	9.74	10.52	17.54	13.51	10.17	11.93	9.63
12-Strip	Theoretical (mm)	12.38	12.46	11.60	9.89	8.78	11.39	9.35	8.98	9.43	7.86	8.75	9.24
Poles	FEM Analysis (mm)	9.97	9.25	11.73	8.39	6.84	9.37	9.80	9.41	9.89	8.21	9.16	9.68

Table 4.8. Comparison between the deflection values obtained from the theoretical analysis and the values predicted by the finite element method of the full-size, composite poles subjected to the same load for both test methods.

	Strip Thickness (cm)	**1.91**	**1.91**	**2.86**	**2.86**	**3.81**	**3.81**
	Load (N)	133	133	133	133	133	133
9-Strip Poles	Theoretical (cm)	12.03	8.28	8.16	7.80	9.65	9.06
	FEM Test (cm)	12.31	8.83	8.27	7.94	9.84	9.23
12-Strip Poles	Theoretical (cm)	9.89	8.03	8.36	7.73	7.73	5.97
	FEM Test (cm)	9.13	8.80	8.43	8.56	7.89	6.83

Table 4.9. Comparison between the maximum bending stress values obtained in the theoretical analysis and predicted by the finite element method of small-scaled composite poles.

	Strip Thickness (cm)	**1.0**			**1.5**			**2.0**			**2.5**		
	Samples	1	2	3	1	2	3	1	2	3	1	2	3
6-Strip	Theoretical (MPa)	58.71	59.84	58.35	63.61	59.14	74.99	86.16	75.35	70.88	92.05	93.40	93.76
Poles	FEM Analysis (MPa)	63.19	63.21	60.65	63.99	60.29	70.92	86.08	76.48	70.81	92.91	94.99	93.35
9-Strip	Theoretical (MPa)	48.35	46.73	44.72	64.60	65.69	63.78	69.14	71.62	69.74	86.56	84.86	93.26
Poles	FEM Analysis (MPa)	49.51	47.16	46.33	67.21	69.29	69.04	71.31	67.57	69.01	88.07	84.19	95.72
12-Strip	Theoretical (MPa)	44.10	33.30	44.30	55.45	44.05	52.09	84.91	75.82	72.93	92.91	69.57	89.78
Poles	FEM Analysis (MPa)	47.21	35.81	47.28	57.88	47.25	53.14	85.98	77.36	73.77	95.58	70.35	89.80

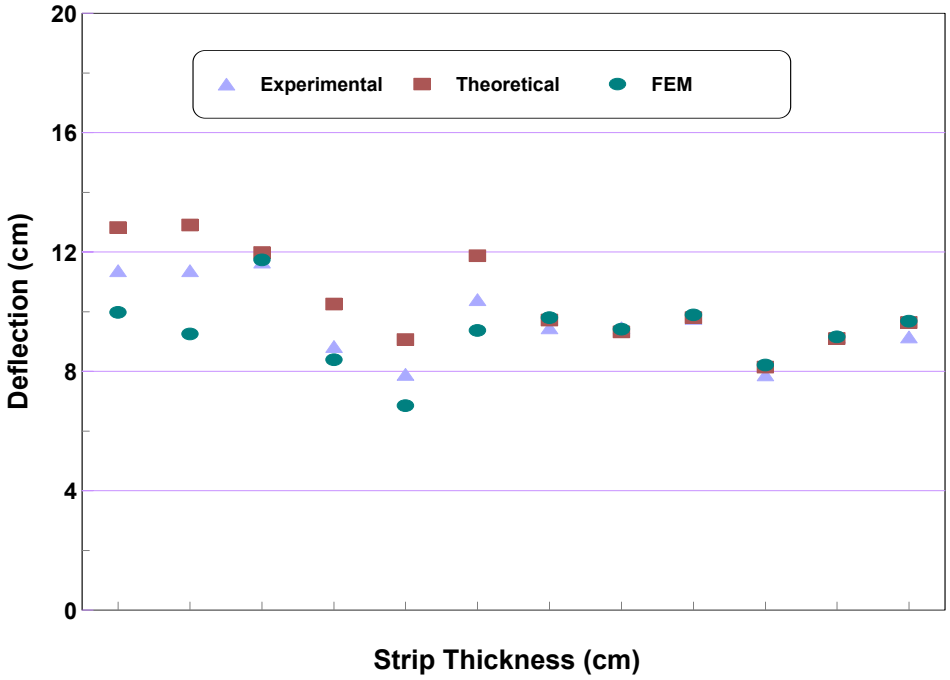

Figure 4.9 Variation of deflection among the experimental, theoretical, and finite element values for the small-scale composite poles with 12 strips.

Table 4.10. Comparison between the deflection values obtained in the experiment and values predicted from finite element analyses of small-scale poles (1.0 cm and 1.5 cm thickness) subjected to a 89 N (20 lbs) load.

	Strip Thickness (cm)	**1.0**			**1.5**		
	Samples	1	2	3	1	2	3
6-Strip	Experiment (mm)	6.93	7.88	8.32	4.92	9.83	10.20
Poles	FEM Analysis (mm)	6.41	7.15	7.84	4.54	9.63	9.70
9-Strip	Experiment (mm)	7.56	8.51	7.56	5.07	5.06	4.35
Poles	FEM Analysis (mm)	7.30	7.89	6.94	4.96	4.56	3.90
12-Strip	Experiment (mm)	5.35	5.37	5.39	4.10	3.52	4.76
Poles	FEM Analysis (mm)	5.25	5.20	4.92	4.16	3.69	4.80

APPENDIX:

DETAIL DERIVATION OF THE THEORETICAL ANALYSIS

This section gives some detail derivation and solutions of the theoretical analyses in Chapter 3. The derivation starts from Equation 17 in Chapter 3 at Page 50. Integrate the first term on the left hand side of Equation 17 in Chapter 3, we have

$$k_8 \int_0^L 2\frac{d^2w}{dx^2}\delta\left(\frac{d^2w}{dx^2}\right)dx$$

$$= 2k_8\left[\frac{d^2w}{dx^2}\delta\left(\frac{dw}{dx}\right) - \frac{d}{dx}\left(\frac{d^2w}{dx^2}\right)\delta w\right]_0^L + 2k_8\int_0^L \frac{d^2}{dx^2}\left(\frac{d^2w}{dx^2}\right)\delta w dx \tag{1}$$

Integrate the second term on the left hand side of Equation 17, we obtain

$$2k_9 \int_0^L \frac{d^3w}{dx^3}\delta\left(\frac{d^3w}{dx^3}\right)dx$$

$$= 2k_9\left[\frac{d^3w}{dx^3}\delta\left(\frac{d^2w}{dx^2}\right) - \frac{d}{dx}\left(\frac{d^3w}{dx^3}\right)\delta\left(\frac{dw}{dx}\right) + \frac{d^2}{dx^2}\left(\frac{d^3w}{dx^3}\right)\delta w\right]_0^L - 2k_9\int_0^L \frac{d^2}{dx^2}\left(\frac{d^3w}{dx^3}\right)\delta w dx \tag{2}$$

Substitute Equations 1 and 2 into Equation 17 in Chapter 3 and rearrange, we obtain the following equation

$$\int_0^L [k_9 \frac{d^6 w}{dx^6} + k_8 \frac{d^4 w}{dx^4} - p_0]\delta w dx +$$

$$[(k_8 \frac{d^2 w}{dx^2} - k_9 \frac{d^4 w}{dx^4})\delta(\frac{dw}{dx})]_0^L + [(k_9 \frac{d^5 w}{dx^5} - k_8 \frac{d^3 w}{dx^3})\delta w]_0^L \quad (3)$$

$$+[(k_9 \frac{d^3 w}{dx^3})\delta(\frac{d^2 w}{dx^2})]_0^L - \frac{1}{2} P\delta w(L) = 0$$

Thus, we obtain one governing equation

$$k_9 \frac{d^6 w}{dx^6} + k_8 \frac{d^4 w}{dx^4} - p_0 = 0 \quad (4)$$

and boundary conditions

$$[k_9 \frac{d^5 w}{dx^5} - k_8 \frac{d^3 w}{dx^3})]_{x=L} = \frac{P}{2} \quad (5)$$

$$(k_8 \frac{d^2 w}{dx^2} - k_9 \frac{d^4 w}{dx^4})|_{x=L} = 0 \quad (6)$$

$$k_8 \frac{d^3 w}{dx^3}|_{x=0} = 0 \quad (7)$$

Equation 4 is a non-homogenous equation, and the solution of the equation is composed of two parts:

$$w = w_c + w_p \quad (8)$$

where w_c is the solution of the complementary function

$$k_9 \frac{d^6 w}{dx^6} + k_8 \frac{d^4 w}{dx^4} = 0 \quad (9)$$

and w_p is any particular solution of Equation 4. Using the differential operator, Equation 9 becomes

$$(k_9 D^6 - k_8 D^4)w = 0 \tag{10}$$

and the roots are

$$m = 0,0,0,0,\sqrt{\frac{k_8}{k_9}},-\sqrt{\frac{k_8}{k_9}} \tag{11}$$

Thus,

$$w = c_1 + c_2 x + c_3 x^2 + c_4 x^3 + c_5 e^{k_{10} x} + c_6 e^{-k_{10} x} \tag{12}$$

where

$$k_{10} = \sqrt{\frac{k_8}{k_9}}$$

and c_1 to c_6 are constants.

For the w_p, it is easily found that

$$w_p = \frac{1}{48 k_8} p_0 x^4$$

is one of the solutions of Equation 4, and the general solution is of the form

$$w = c_1 + c_2 x + c_3 x^2 + c_4 x^3 + \frac{1}{48 k_8} p_0 x^4 + c_5 e^{k_{10} x} + c_6 e^{-k_{10} x} \tag{13}$$

We may find c_1 to c_6 using boundary conditions. The derivatives of Equation 12 are as followings

$$w' = C_2 + 2C_3x + 3C_4x^2 + \frac{1}{12k_8}p_0x^3 + C_5k_{10}e^{k_{10}x} - C_6k_{10}e^{-k_{10}x}$$

$$w'' = \quad 2C_3 \; + 6C_4x \; + \frac{1}{4k_8}p_0x^2 \; + C_5k_{10}^2e^{k_{10}x} + C_6k_{10}^2e^{-k_{10}x}$$

$$w''' = \qquad\quad +6C_4 \quad + \frac{1}{2k_8}p_0x \; + C_5k_{10}^3e^{k_{10}x} - C_6k_{10}^3e^{-k_{10}x} \tag{14}$$

$$w^{IV} = \qquad\qquad \frac{1}{2k_8}p_0 \quad + C_5k_{10}^4e^{k_{10}x} + C_6k_{10}^4e^{-k_{10}x}$$

$$w^{V} = \qquad\qquad\qquad\qquad C_5k_{10}^5e^{k_{10}x} - C_6k_{10}^5e^{-k_{10}x}$$

Substitute Equation 14 into boundary conditions and c_1 to c_6 may be solved:

$w|_{X=0} = 0$

$$C_1 + C_5 + C_6 = 0 \tag{15}$$

$w'|_{x=0} = 0$

$$C_2 + k_{10}C_5 - k_{10}C_6 = 0 \tag{16}$$

$k_8 \frac{d^3w}{dx^3}|_{x=0} = 0$

$$6C_4 + C_5k_{10}^3 - C_6k_{10}^3 = 0 \tag{17}$$

$EIw''|_{x=L} = 0$

$$2C_3 + 6C_4L + \frac{1}{4k_8}p_0L^2 + C_5k_{15}^2e^{k_{15}L} + C_6k_{15}^2e^{-k_{15}L} \tag{18}$$

$(k_8 \frac{d^2w}{dx^2} - k_9 \frac{d^4w}{dx^4})|_{x=L} = 0$

$$\frac{p_0}{2k_8} + C_5k_{15}^4e^{k_{15}L} + C_6k_{15}^4e^{-k_{15}L} = 0 \tag{19}$$

$$[k_9 \frac{d^5 w}{dx^5} - k_8 \frac{d^3 w}{dx^3})]_{x=L} = \frac{P}{2}$$

$$k_8(6C_4 + \frac{p_0 L}{2k_8} + C_5 k_{10}^3 e^{k_{10}L} - C_6 k_{10}^3 e^{-k_{10}L}) - k_9(C_5 k_{10}^5 e^{k_{15}L} - C_6 k_{10}^5 e^{-k_{15}L}) + \frac{p}{2} = 0 \quad (20)$$

Solve Equations 15 to 20, the coefficients are obtained:

$$C_1 = \frac{k_{10}(p_0 L + P)(e^{k_{10}L} - e^{-k_{10}L}) + 2p_0}{2k_8 k_{10}^4 (e^{k_{10}L} + e^{-k_{10}L})}$$

$$C_2 = -\frac{p_0 L + P}{2k_8 k_{10}^2}$$

$$C_3 = \frac{p_0 L^2 + 2PL}{8k_8} + \frac{p_0}{2k_8 k_{10}^2}$$

$$C_4 = -\frac{p_0 L + P}{12k_8}$$

$$C_5 = \frac{k_{10}(p_0 L + P)e^{-k_{15}L} - p_0}{2k_8 k_{10}^4 (e^{k_{10}L} + e^{-k_{10}L})}$$

$$C_6 = -\frac{k_{10}(p_0 L + P)e^{-k_{15}L} + p_0}{2k_8 k_{10}^4 (e^{k_{10}L} + e^{-k_{10}L})}$$

VITA

The author was born in Shuang Yang (a special district of Chang Chun, the capital city of Jilin Province), China. He received a Bachelor's degree in wood science and technology from Northeast Forestry University in China in 1987. He received a Master of Science degree in wood composites from the same University in 1990. He was employed by the Research Institute of Heilongjiang Forest Products Industry as an engineer from 1990 to 1996. He earned the second Master of Science degree in forestry from Louisiana State University in 1998. He is presently a candidate for the doctoral degree in forestry, with an emphasis on wood science and technology.